NASA CONTRACTOR REPORT

NASA CR-253

NASA CR-253

DISTRIBUTION STATEMENT A
Approved for public release
Distribution Unlimited

19960506 030

DEVELOPMENT OF A RADIO-FREQUENCY TRANSPARENT ENERGY-ABSORBING STRUCTURAL ELEMENT

by Ronald H. Smith

Prepared under Contract No. NAS 1-3906 *by*
NORTHROP CORPORATION
Newbury Park, Calif.

for

DTIC QUALITY INSPECTED 1

NATIONAL AERONAUTICS AND SPACE ADMINISTRATION • WASHINGTON, D. C. • JULY 1965

DEPARTMENT OF DEFENSE
PLASTICS TECHNICAL EVALUATION CENTER
PICATINNY ARSENAL, DOVER, N. J.

NASA CR-253

DEVELOPMENT OF A RADIO-FREQUENCY TRANSPARENT ENERGY-ABSORBING STRUCTURAL ELEMENT

By Ronald H. Smith

Distribution of this report is provided in the interest of information exchange. Responsibility for the contents resides in the author or organization that prepared it.

Prepared under Contract No. NAS 1-3906 by
NORTHROP CORPORATION
Newbury Park, Calif.

for

NATIONAL AERONAUTICS AND SPACE ADMINISTRATION

For sale by the Clearinghouse for Federal Scientific and Technical Information
Springfield, Virginia 22151 — Price $4.00

BEST QUALITY AVAILABLE

DEVELOPMENT OF A RADIO-FREQUENCY TRANSPARENT

ENERGY-ABSORBING STRUCTURAL ELEMENT

ABSTRACT

An experimental investigation has been conducted to develop highly efficient energy-absorbing structural elements from radio-frequency transparent materials. The materials were evaluated using two types of energy absorption processes; the fragmenting tube and the crushing of honeycomb and foamed materials. Plastic reinforced glass fabric tubes, employed in the fragmenting tube process, yielded specific energies of 28,400 and 12,300 ft-lb/lb for fabric orientation in the longitudinal and hoop directions respectively. The crushing of nylon-phenolic honeycomb yielded a value of specific energy of 14,400 ft-lb/lb for a 3/16 inch cell size, 9.0 lb/ft^3 density, and with a usable stroke of 80% of initial length. Radio frequency transmission losses were well within acceptable limits for the specified 100 to 2000 megacycle frequency range investigated.

FOREWORD

The final report, prepared in accordance with the requirements of Contract No. NAS 1-3906, covers analytical studies and experimental tests performed during the period 1 June 1964 through 31 January 1965. The work was sponsored by the National Aeronautics and Space Administration, Langley Research Center, with technical guidance provided by NASA Project Monitor, Mr. J. McGehee.

This program at Northrop Ventura was under the cognizance of Mr. W. R. Stoeltzing, Project Manager, and Mr. R. H. Smith, Project Engineer. Acknowledgement is extended by the author to W. F. De Mario, R. D. Wanselow, and D. C. Borgman for assistance in this program, respectively, in fabrication and testing of elements, electrical testing and analysis, and the tabulation and analysis of results.

CONTENTS

ILLUSTRATIONS

TABLES

SUMMARY

An investigation was made to determine the efficiency of radio frequency transparent material deformation type energy absorption structural elements applicable to spacecraft landing systems. Requirements limited efficiencies to values greater than 10,000 ft-lb/lb of material and impact load factors ranging from 50 to 1000 earth g-units. Preliminary investigations were conducted on the highly efficient process of tube fragmenting over a die using unreinforced and reinforced plastic tubes. Tests were also conducted on the crushing of nylon phenolic honeycomb of several cell sizes, syntactic foam and nylon phenolic honeycomb.

The results indicated the same high efficiency for reinforced plastic tubes as had been shown for aluminum tubes fragmented over steel dies. The most efficient tube was tape wrapped using longitudinally oriented 143 E glass fabric and an epoxy resin system. The orientation of the fabric is significant resulting in efficiencies of 28,400 and 12,300 ft-lb/lb of material for longitudinal and hoop direction orientations, respectively. The bi-directional 181 fabric with the same resin system produced more reliable results with an efficiency of 23,800 ft-lb/lb of material without splitting as occurred in 143 fabric tubes. Another highly efficient structural element is 3/16-in. cell-size nylon phenolic honeycomb, which tested to values of 14,400 ft-lb/lb of material, for 80% usable stroke. In both the tube and honeycomb elements an ideal load stroke graph was produced by the tests with no initial peaking and no sharp oscillations of the load with stroke for full deformation. Radio frequency transparency evaluations for crushed and uncrushed elements established that the fragmented tube and crushed honeycomb processes were the lowest in transmission loss and were well within acceptable limits for the specified 100 to 2000 megacycle frequency range investigated.

INTRODUCTION

Energy absorption systems which are reusable, such as shock absorbers, springs, and other systems, have been in use for a considerable period of time. The more stringent requirements for energy absorption systems used in the landing impact of spacecraft have resulted in intensive research in single-application energy absorption systems which meet weight, volume, and environment limitations. Additional requirements for landing systems now include the transmission of radio frequency signals through the energy absorption system before and after landing impact.

Single application energy absorption systems which have been investigated for spacecraft landing use include: the compression of a gas in landing bags; the acceleration of a fluid or other mass; friction devices; chemical energy; and the mechanical deformation of material or structure. One of the most efficient processes in the mechanical deformation category is the energy absorption system which employs frangible metal tubing as the working element. Other mechanical deformation systems of interest are crushable honeycomb elements and crushable foam materials. These three types of mechanical deformation systems; i.e., the fragmenting of a tube, the crushing of honeycomb, and the crushing of foam material, have been evaluated in this program, considering non-metallic materials which are radio frequency (rf) transparent before and after crushing.

The principal objective of this program effort has been the development of efficient energy absorbing structural elements which are rf transparent before and after crushing. The three element types to be investigated are the nonmetallic tubes, honeycomb, and foams according to the following requirements:

1. The structural characteristics shall be predictable and reproducible.

2. The specific energy obtained from the material through the energy-absorbing process shall be a minimum of 10,000 ft-lb/lb.

3. The ability of the process to accommodate varying sizes shall be demonstrated and the variation of the force supplied by the process with geometric and material parameters shall be determined.

4. The method of fabrication of the energy-absorbing elements shall be defined.

5. An analysis shall be accomplished of the energy-absorption process for determining, within engineering accuracy, the force supplied by the process as a function of the pertinent parameters.

6. The radio frequency range of interest in this application is 100 megacycles to 2000 megacycles.

7. The material employed shall have a dielectric constant within the range of 1.0 to 10.0 and a loss tangent within the range of 0.03 to 0.05.

8. The load range of interest depends upon the particular application and it is felt that many applications would be encompassed by objective 3 of these requirements. However, loads from 50 to 1000 earth g-units would have considerable application.

SYMBOLS

E_{sp} = Specific energy, ft-lb/lb

D = Tube diameter, in.

t = Tube thickness, in.

r = Forming radius of die, in.

w = Element weight, lb

L = Element length, in.

C = End fixity

k_f = Shape parameter

P = Axial load, lb.

δ = Displacement, in.

E = Young's modulus, psi

μ = Poisson's ratio

G = Shear modulus, psi

e = Strain, in/in.

F_f = Fragmenting stress, ksi

$\bar{F}_{cc}$ = Average crushing stress, ksi

F_{tu} = Ultimate tensile stress, ksi

F_{cu} = Ultimate compressive stress, ksi

F_{su} = Ultimate shear stress, ksi

t_f = Honeycomb foil gage thickness, in.

s = Honeycomb cell size, in.

K = Honeycomb geometric folding parameter

ρ = Material density, lb/ft^3

ρ_c = Honeycomb core density, lb/ft^3

A = Required honeycomb area, in^2

$\bar{P}$ = Average crushing load, lb.

V = Volume of element, in^3

a = Acceleration, ft/sec^2

m = Vehicle mass, slugs

W = Vehicle weight, lb.

V_n = Impact velocity, ft/sec

n_x = Impact load factor acting along flight path axis, g's

L' = Usable stroke, in.

N = Number of tubes

ϕ = Spherical angle of impact absorption material effectiveness, degrees

L_s = Sample radio frequency insertion loss, db

P_i = Input power level, dbm

P_o = Output power level, dbm

P_r = Reflected power level, dbm

ϵ^* = Relative absolute complex dielectric constant

ϵ' = Real relative dielectric constant

ϵ'' = Relative loss factor

$\tan \delta$ = Loss tangent

Q = Quality factor

λ_o = Operating wavelength, meter

ϵ_m = Relative compound dielectric constant of a mixture of two materials

MATERIALS SELECTION

General Considerations. - The efficiency of a material-deformation-type of energy absorption process is a function of material properties and element geometry. There are three types of elements which are considered in this evaluation: the frangible tube, the crushable honeycomb, and the crushable foams. Selection of materials for each of these types of elements requires an evaluation of detail geometric variables: 1) in the tube fragmenting process, 2) the honeycomb crushing and folding of the cell walls, and 3) the foam crushing or crumbling characteristics. This program has two primary requirements for these types of elements which limit the use of effective materials and processes which have been used before; they are a specific energy absorbing capability of 10,000 ft-lb/lb minimum, and a radio frequency transparency between specified limits before and after the elements have been used for energy absorption.

A review of previous investigations in mechanical deformation elements provided some indication of material mechanical properties desired in the rf-transparent elements. Figure 1 compares the relative efficiency of mechanical deformation types of energy-absorption systems based on previous investigations. The 2024-T3 aluminum alloy tubing material when fragmented over a die is shown to be the most efficient, with a value of 31,000 ft-lb/lb. The tube fragmenting process is shown to be much more efficient than the most frequently used single-application type structural elements such as balsa wood, aluminum honeycomb, or pressurized thin-walled metallic cylinders. This high tube-fragmenting efficiency is achieved by working the 2024-T3 material to 90% of the compressive yield. Other limiting parameters for the tube are a diameter/wall thickness ratio which does not cause local crippling of the tube, and column length properties which are not critical. These characteristics would also be a primary consideration in the selection of non-metallic tubing materials.

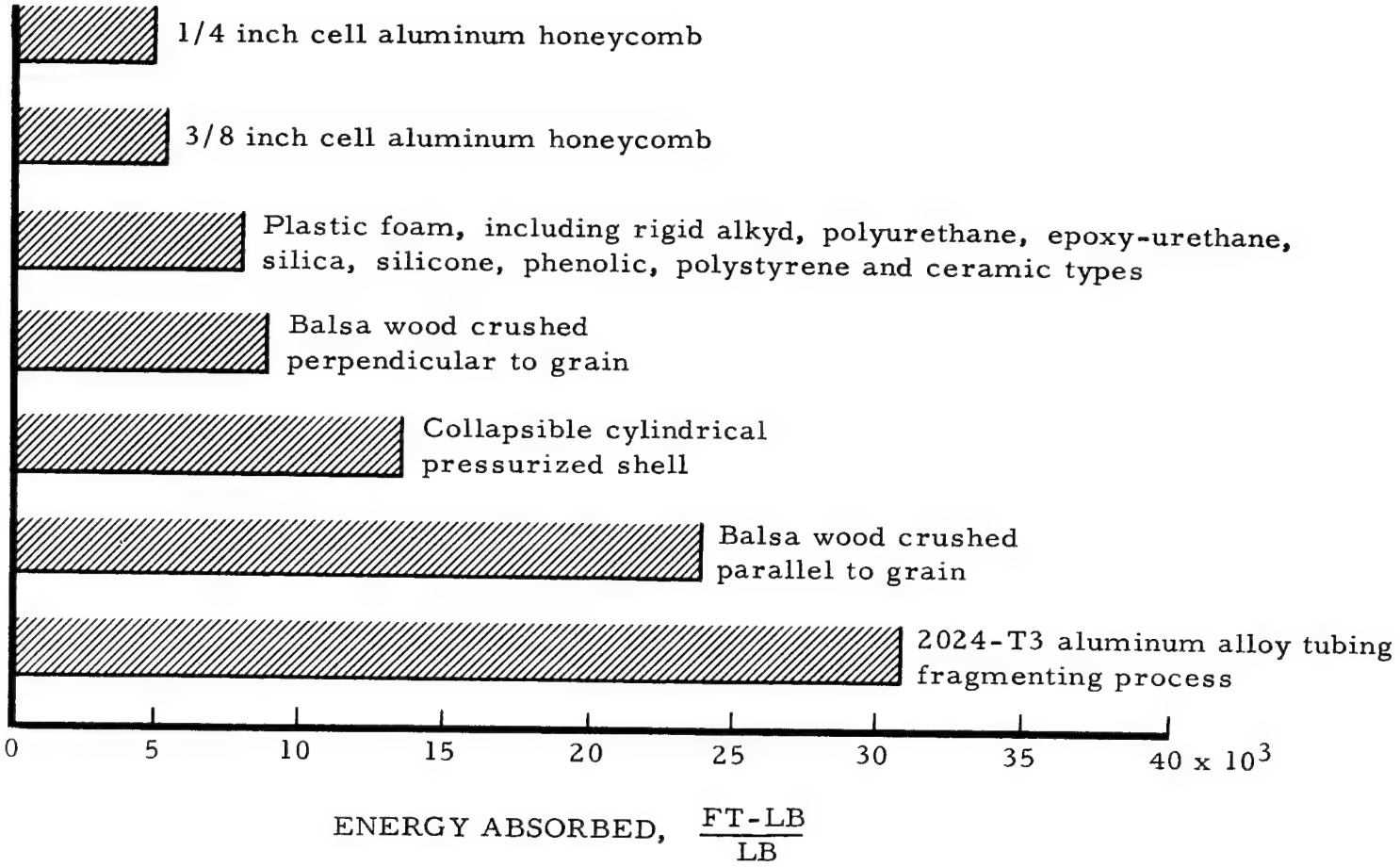

Figure 1. Energy Absorption Capabilities of Various Materials and Processes

The aluminum honeycomb shown in Figure 1 would not qualify for the 10,000 ft-lb/lb efficiency restriction considered in this investigation. Significant parameters for honeycomb crushing have been investigated and have been shown to be the yield strength of the material and the ratio of the core foil gage to the cell size. The smallest cell size for the 3003-H38 honeycomb core material presented is not included in the comparison and would improve the efficiency. The material yield strength of 5052-H38 aluminum alloy core material is 37,000 psi compared to 27,000 psi for the 3003-H38. This material property improvement would result in considerable efficiency improvement and is a primary consideration in the selection of non-metallic honeycomb core materials. The foam efficiency curves are also shown to be below the minimum 10,000 ft-lb/lb requirement; however, new types of foam are available with considerable increase in crushing strength efficiency.

An important additional consideration in energy absorption elements development is the shape of the load deformation curve. An ideal shape is a uniform load with deformation; i.e., a rectangular shaped graph. The actual shape of the three element types to be considered in this program is presented for fragmented aluminum tubes, crushed aluminum honeycomb, and crushed polyurethane foam in Figure 2 based on the results of previous investigators. The highly efficient 2024-T3 aluminum alloy tubing is shown to have an initial sharp peak force which is up to one third more than the average fragmenting force. The actual fragmenting force over the full range of deformation is an oscillating value not shown in the graph. Figure 2 also shows that a tapered wall thickness at the end of the tube alters this initial peak force, and that pre-fragmenting the end of the tube also reduces this peak force, but both of these methods cause a loss in total load stroke area. An additional characteristic of the fragmenting tube which is shown by these curves is that it may be fragmented for its full length.

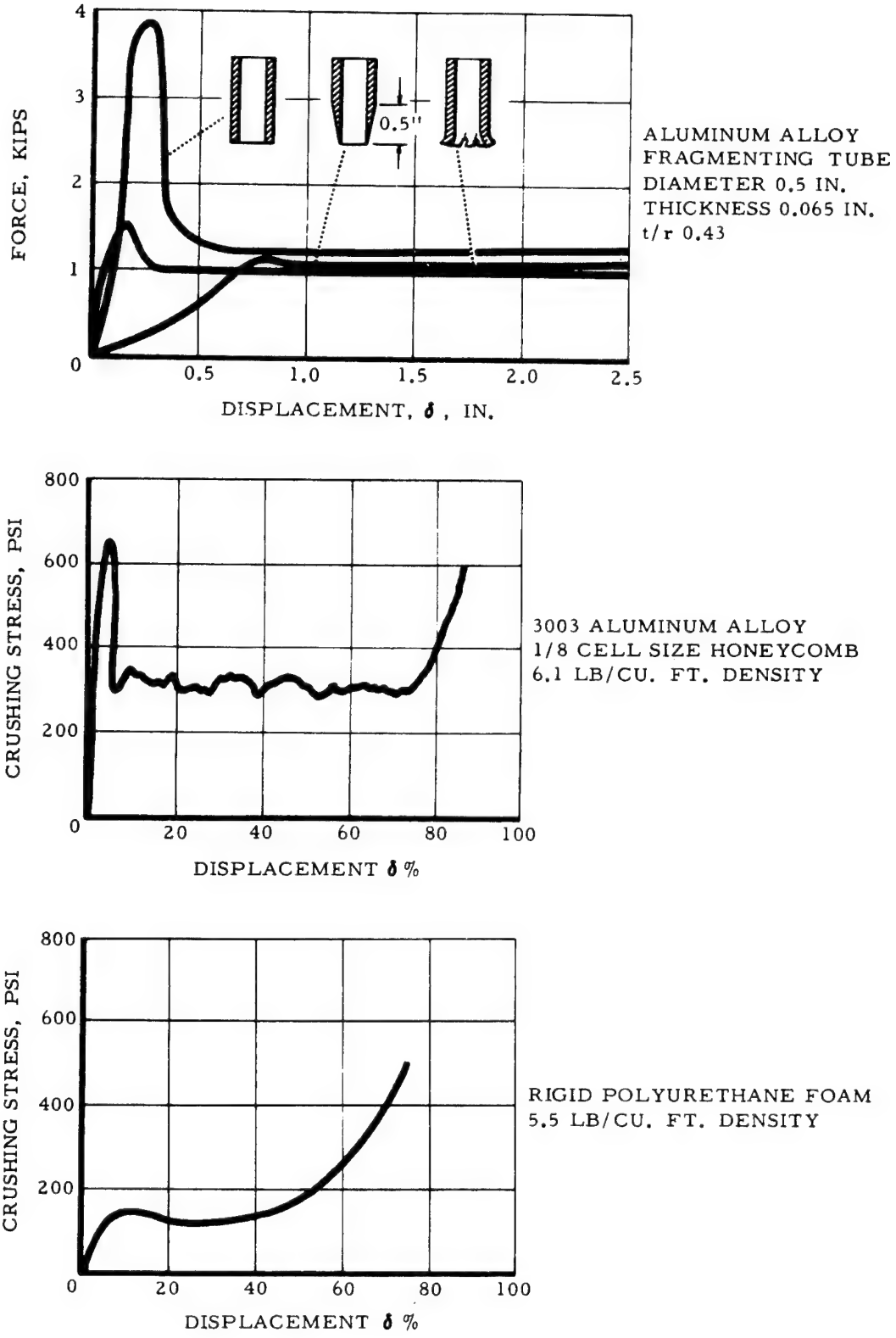

Figure 2. Typical Non Radio Frequency Transparent Energy Absorption Load Displacement Graphs

The aluminum honeycomb curve also has an initial peak stress which is twice the average crushing stress; this too can be removed by pre-crushing. There are smaller fluctuations in crushing stress than in the tube fragmenting load fluctuation for the entire stroke except for a peaking of stress again at 75% of the total honeycomb element length; this results in a usable stroke limitation for honeycomb.

The foam element load deformation shape requires a reasonably high stress level before the material yields to a constant stress with deformation until about 60% of the total length is reached at which point the stress begins to rapidly rise to a "solid height" value. Foam element load deformation curves are like the honeycomb element curves in that both are limited by an effective length of stroke but the foam curve does not start with a sharp peak.

Candidate RF-Transparent Fragmenting Tube Element Materials. - Candidate materials considered for this program are in two categories: purchased unreinforced plastic tubes and reinforced tubes, and fabricated glass-fiber reinforced plastic tubes. The unreinforced tubes were made from vinyl and high-impact polystyrene. The purchased reinforced tubes consisted of a phenolic resin system with cotton fabric reinforcement. The first glass-fiber-reinforced tubes to be fabricated were with phenolic resin so that a comparison could be made with the purchased cotton-reinforced phenolic tubes. Additional fabricated tubes were made using hand layup methods and polyester resin. Epoxy resin was substituted for a few tubes. Different types of fabric weaves and direction of fabric layup with respect to the hoop and longitudinal direction of the tube were also included in the variety of tubes fabricated.

The selection of a material for tube fragmenting tests which is also capable of meeting the radio frequency transparency requirements limits selection to non-metallics. The most promising of the non-metallic

materials when considered on a strength/density basis are the glass-fiber-reinforced plastic (GRP) laminates. In a discussion of the energy absorption efficiency curves, Figure 1, the 2024-T3 tube material achieved high efficiency by working to 90% of the 42,000 psi compressive yield strength. Table I provides a comparison of the properties of this isentropic aluminum alloy with the most efficient epoxy resin system glass-fiber-reinforced laminate material for two fabric weaves. Since this latter material is orthotropic, strength in the 0 degree and 90 degree directions must be considered and the directional strength at other angles is also important for cross lamination. Figures 3 and 4 present angular strength and stiffness properties for cotton-reinforced phenolic, polyester with glass reinforcement, and epoxy with glass reinforcement for the bi-directional-strength 181 fabric weave and for the unidirectional-strength 143 fabric. The epoxy resin system with 181 fabric reinforcement is shown to have a strength comparable to the 2024-T3 aluminum alloy in compression; however, the density is two thirds that of aluminum alloys.

Also shown in Figures 3 and 4 are the straight-line-type-stress-strain curves and the almost linear tangent modulus curves. These tangent modulus curves for 181 fabric and 143 fabric with an epoxy resin system have been replotted in Figure 5 for comparison with metals. A practical limitation for the geometry of tubes used in tube-fragmenting energy-absorption applications is its Euler column strength which is also dependent on the material tangent modulus. Figure 6 is an optimum column weight efficiency comparison of stable section columns of epoxy resin system GRP columns for two fabric weaves compared with metallic materials. The GRP material is seen to be competitive with the best metallic materials, and therefore column limitations would not be critical for GRP framenting tubes.

Preliminary Fragmenting Tube Tests. - A preliminary fragmenting tube test program was conducted on unreinforced and reinforced non-metallic candidate materials fabricated as tubes in order to indicate the most

TABLE I. MIL-KDBK-17 DATA (WET)
MECHANICAL PROPERTIES OF "E" GLASS AND EPOXY RESIN SYSTEM
AND DATA FOR ALUMINUM TUBING FROM MIL-KDBK-5

Fabric Weave	$\frac{E_x}{10^6}$ (psi)	$\frac{E_y}{10^6}$ (psi)	$\frac{\sqrt{E_x E_y}}{10^6}$ (psi)	$1 - \mu_x \mu_y$	F_{cu_x} (ksi)	F_{cu_y} (ksi)	F_{tu_x} (ksi)	F_{tu_y} (ksi)	F_{su_i} (ksi)	F_{su_e} (ksi)	$\frac{G}{10^6}$ (psi)
181	3.28	3.14	3.21	0.980	45	38.2	45.0	42.4	6.79	14.0	0.810
143	5.12	2.08	3.26	0.972	60	26.3	85.0	10.2	3.69	7.86	0.590
2024-T3 Aluminum	$E_c = 10.7$			0.889	$F_{cy} = 42$		$F_{tu} = 64$		$F_{su} = 39$		4.0

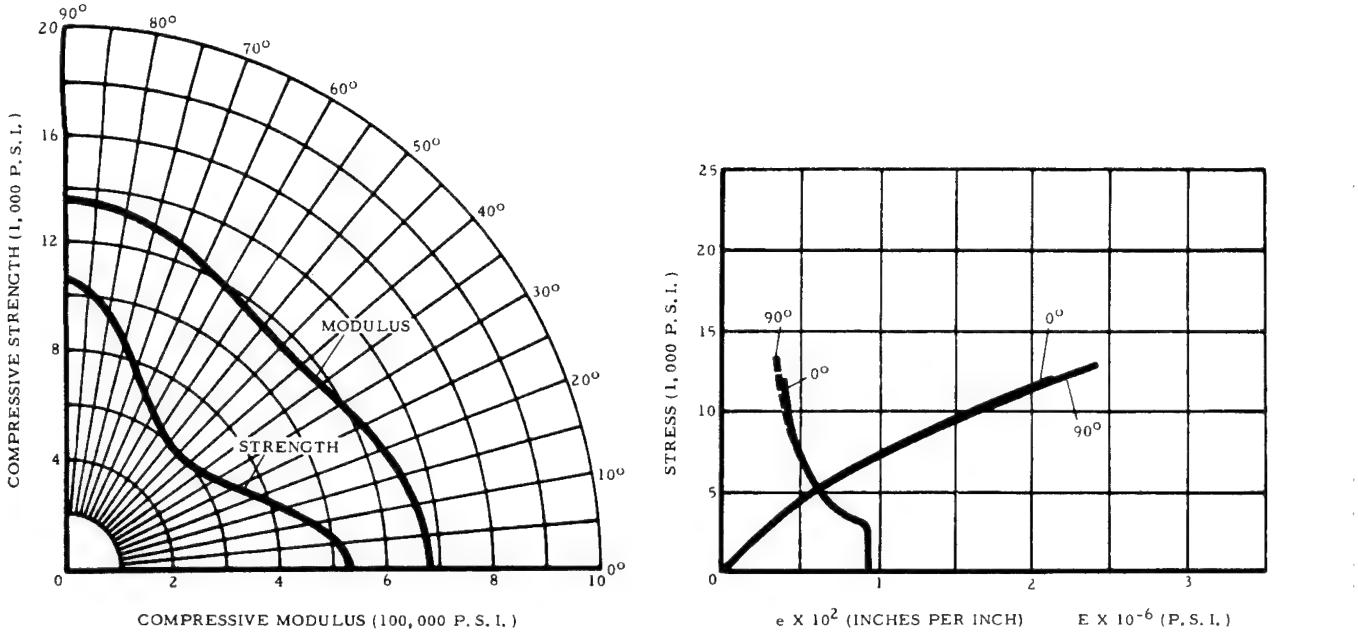

Parallel Laminated Cotton Fabric, Phenolic Resin

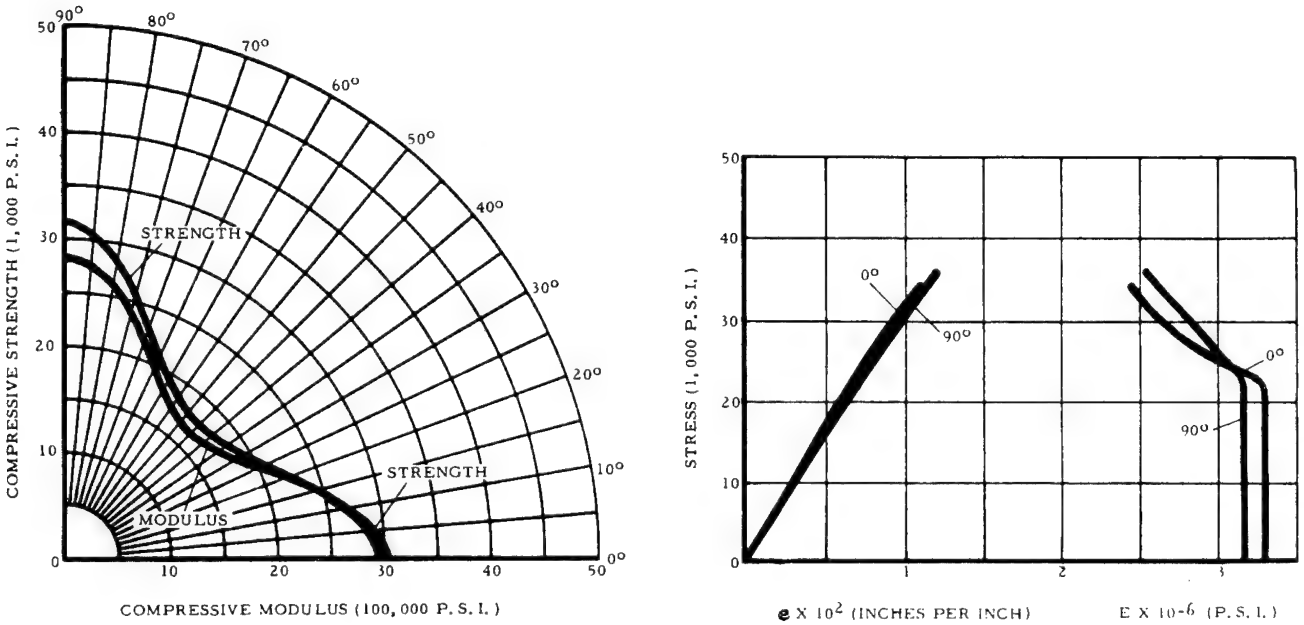

Parallel Laminated 181 Glass Fabric, Polyester Resin

Figure 3. Directional Strength and Stiffness Properties of Reinforced Plastic Laminates Using Resin Systems and Fabrics noted

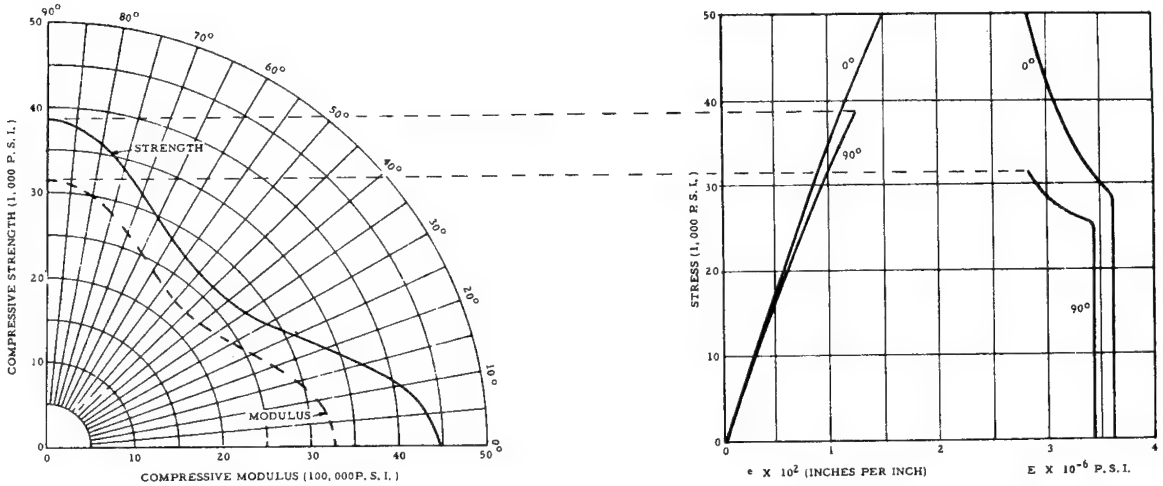

PARALLEL LAMINATED 181 FABRIC

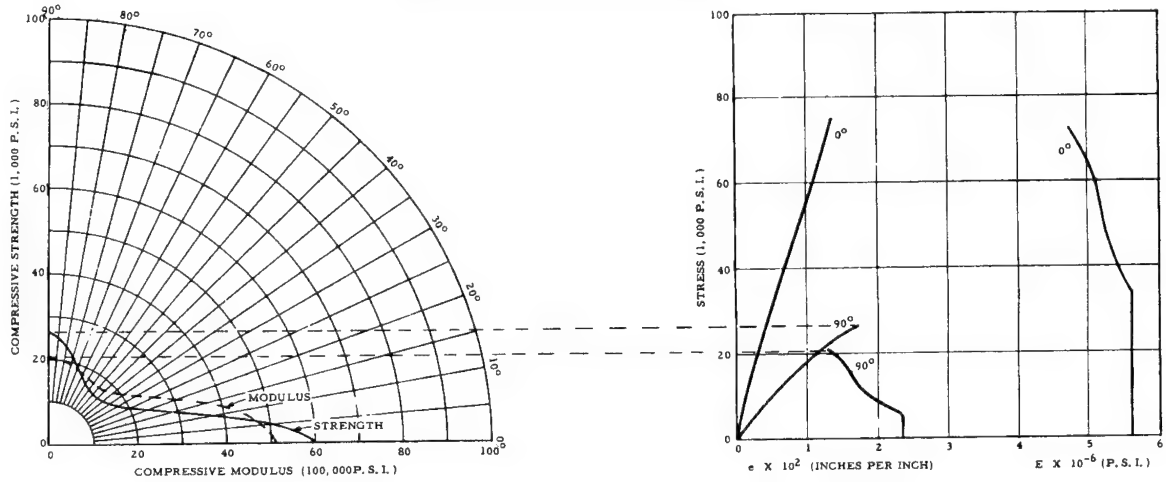

PARALLEL LAMINATED 143 FABRIC

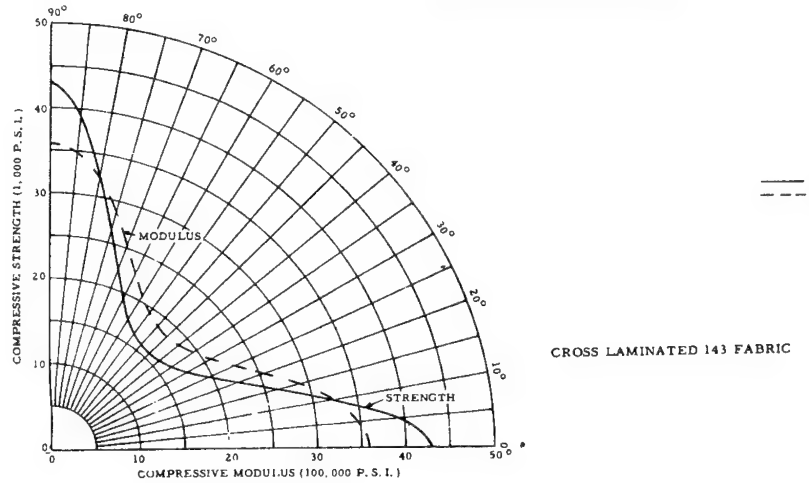

CROSS LAMINATED 143 FABRIC

Figure 4. Directional Strength and Stiffness of Reinforced Plastic Laminates with Epoxy Resin Systems

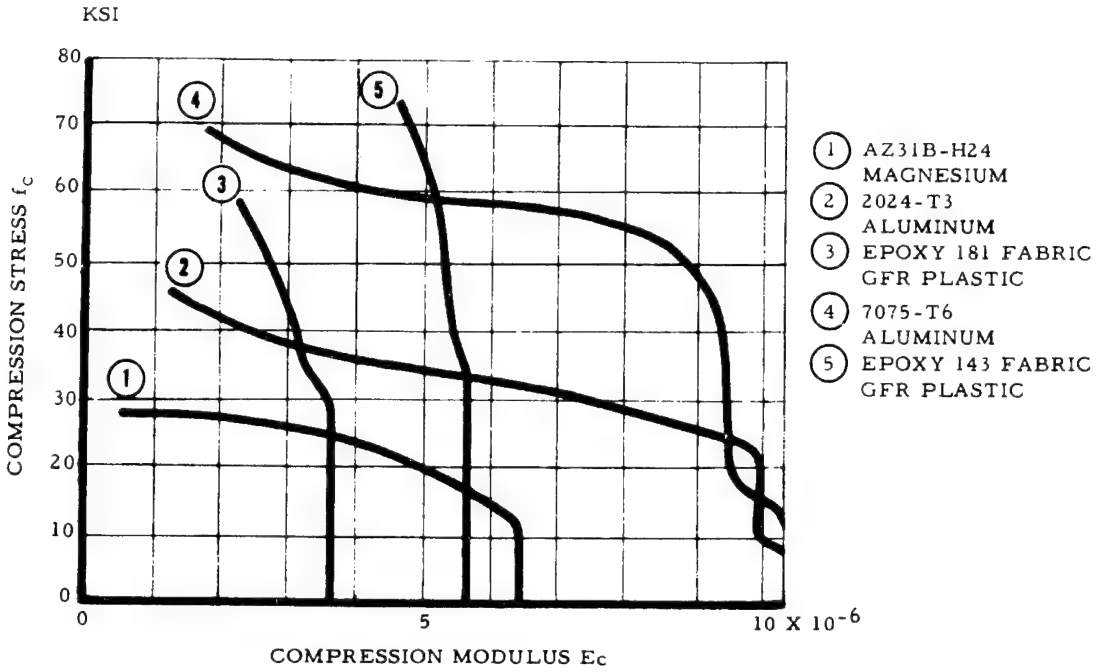

Figure 5. Strength/Stiffness Properties of "E" Glass Epoxy Plastic with 181 and 143 Fabric Compared with Metallic Materials

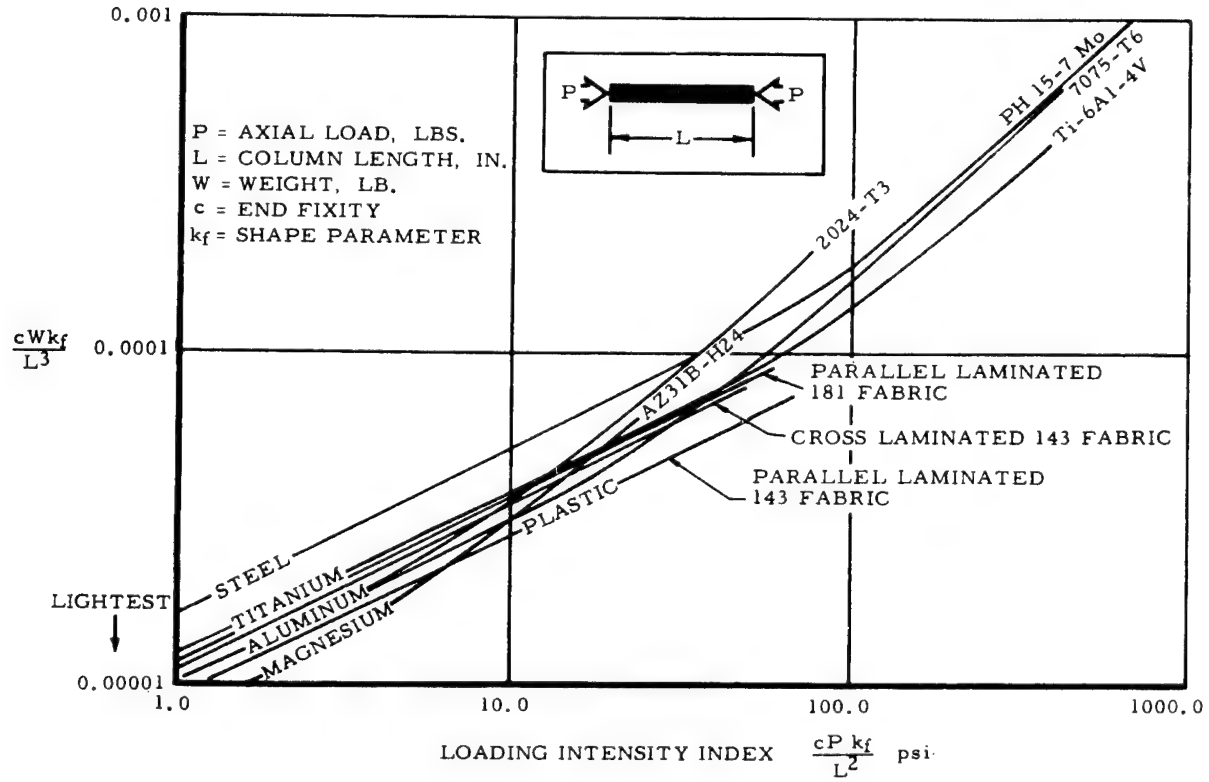

Figure 6. Optimum Column Weight Efficiency Comparisons with Metallic Materials of "E" Glass Epoxy GFR Plastic Using 181 Fabric

promising materials for the program. Figure 7 shows the fragmenting process of a tube on the die for a longitudinally orientated GRP laminate using 143 fabric weave. The dies were fabricated from mild steel or cast from an epoxy resin system to the shape shown in Figure 7. The die guide shaft is one-inch long with the end rounded to eliminate gouging of the tube walls. The diameter of the die is made approximately 0.004 inch smaller than the inside diameter of the tube, and the transition between the shaft and the forming groove section of the die was smooth.

Preliminary test evaluations were conducted on the 12,000-lb capacity universal testing machine at a rate of loading of 1.0 inch per minute. Automatic load deformation plots of each test were recorded and the test specimens were weighed before and after each test to be used in the calculation of the specific energy absorption. Figure 8 shows typical candidate 1.0-inch diameter tubing after tests. The unreinforced tubing has a stress-strain curve shape which is similar to the load deformation graphs for foam materials; i.e., the materials have a definite yield point and a considerable elongation under steady stress until failure. This material characteristic for vinyl as shown resulted in the failure of these tubes to commence fragmenting even when split longitudinally at intervals before testing. The polystyrene material shattered in each test almost as though it were a solid glass tube material. The phenolic resin reinforced with cotton fabric also shattered as shown and repeatedly resisted fragmenting when tests were conducted on the various dies shown in Figure 9. When the hand layup phenolic resin system reinforced with 181 E glass fabric was tested, good fragmenting action was observed. Since polyester material properties are interchangeable with the phenolic resin according to MIL-HDBK-17, further tubing tests were conducted with the lower cost polyester resin system. Figure 10 illustrates the good fragmenting action of a polyester resin system tube reinforced with 181 E glass fabric.

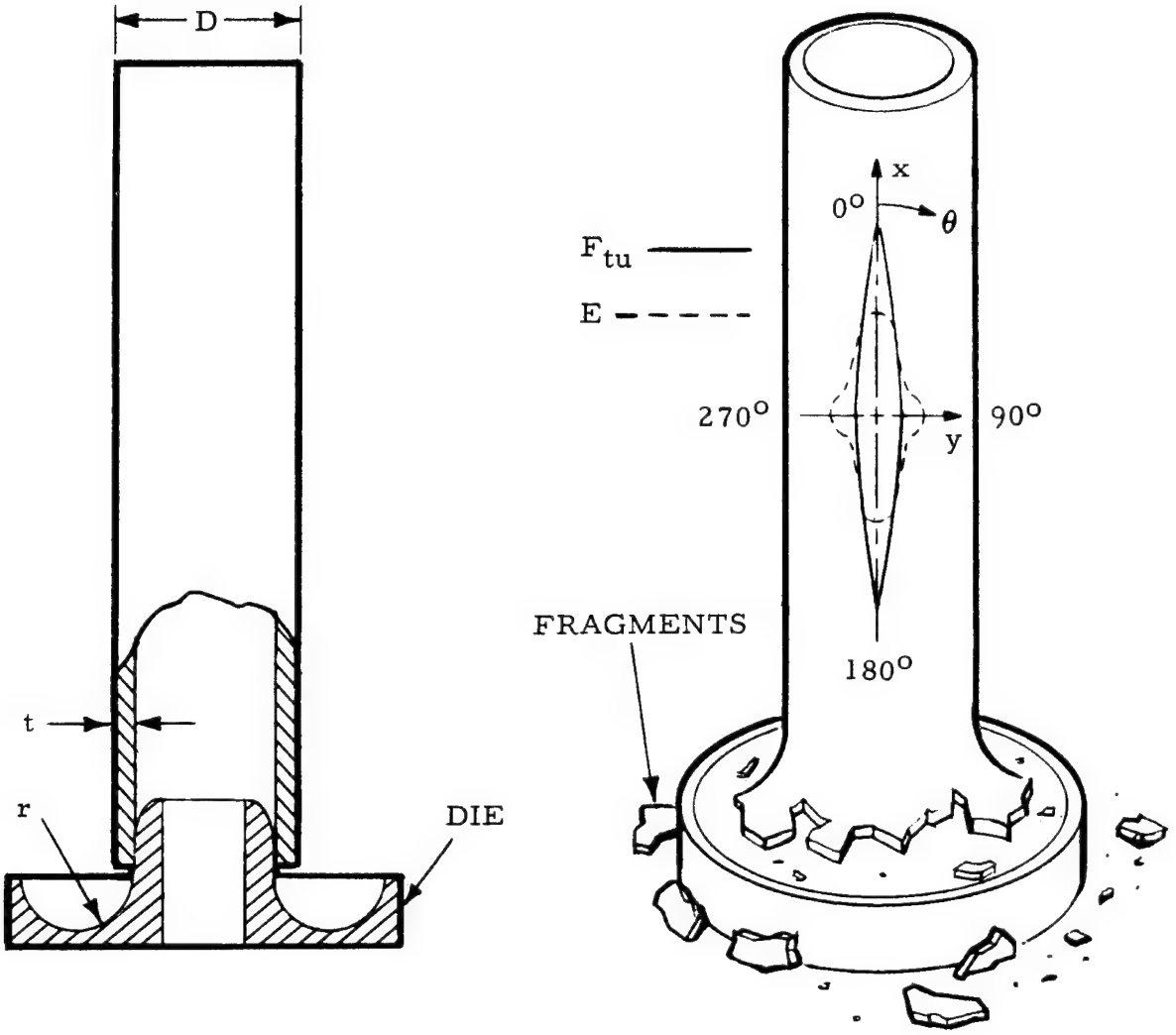

Figure 7. Sketch Illustrating Fragmenting Process for Longitudinally Oriented 143 Glass Fabric Laminated Tubing

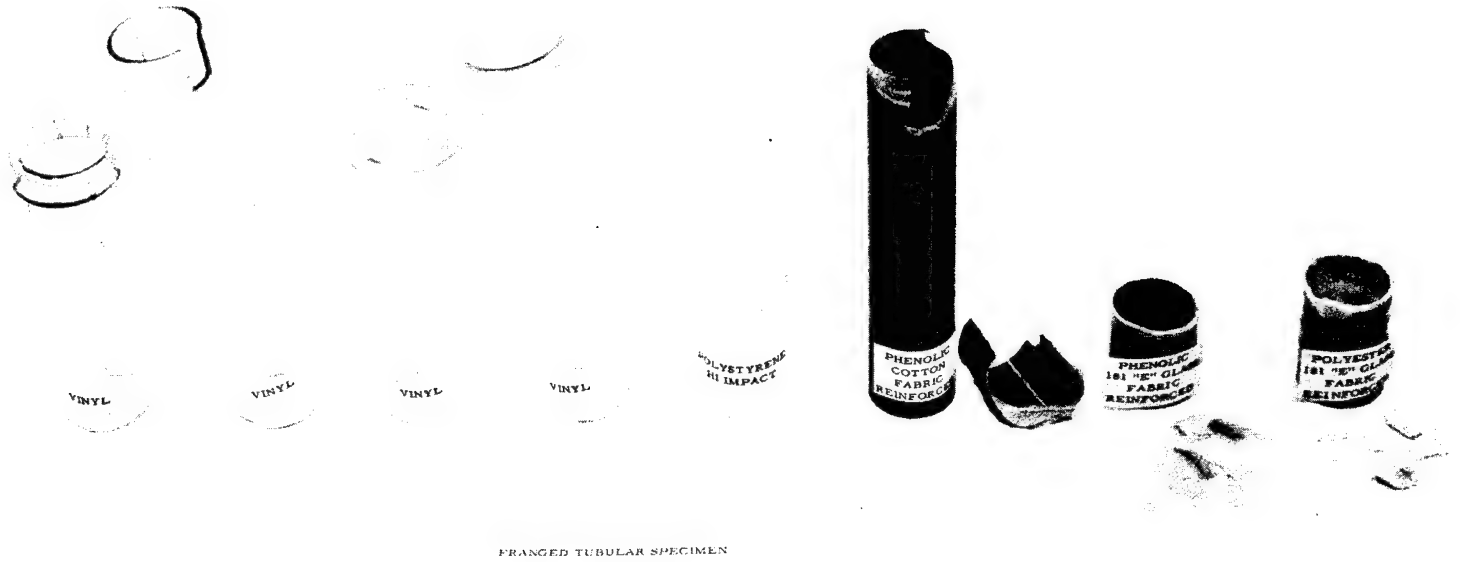

Figure 8. Fragmented Tubes of Various Plastic Materials

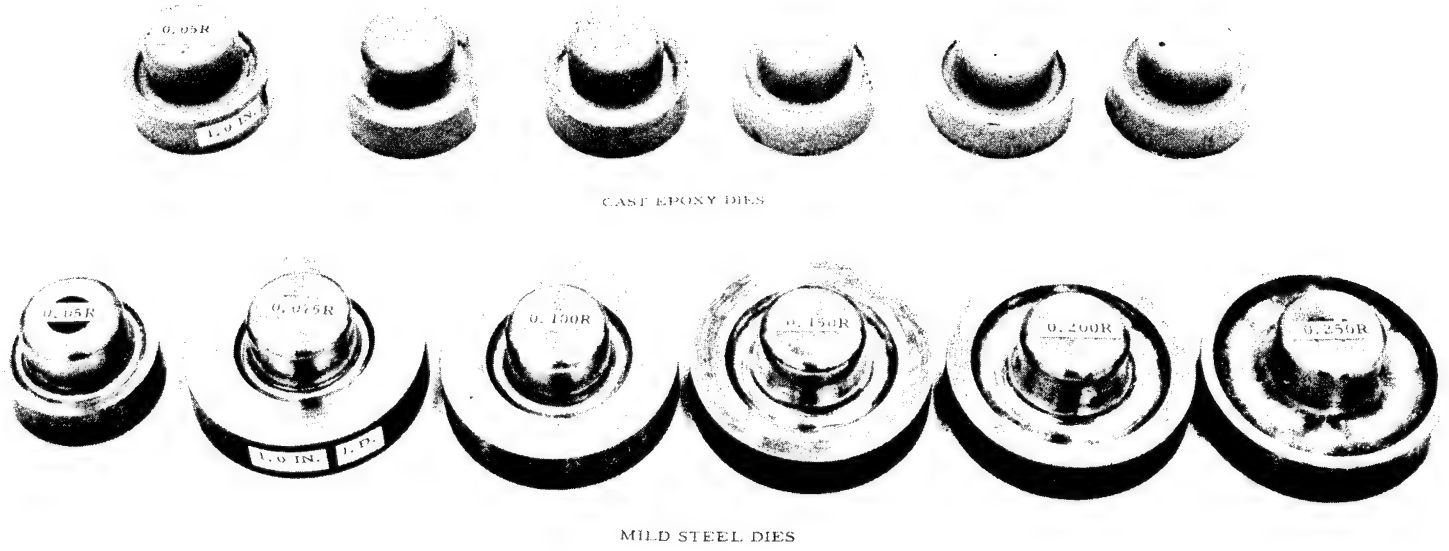

Figure 9. Mild Steel and Cast Epoxy Die Series

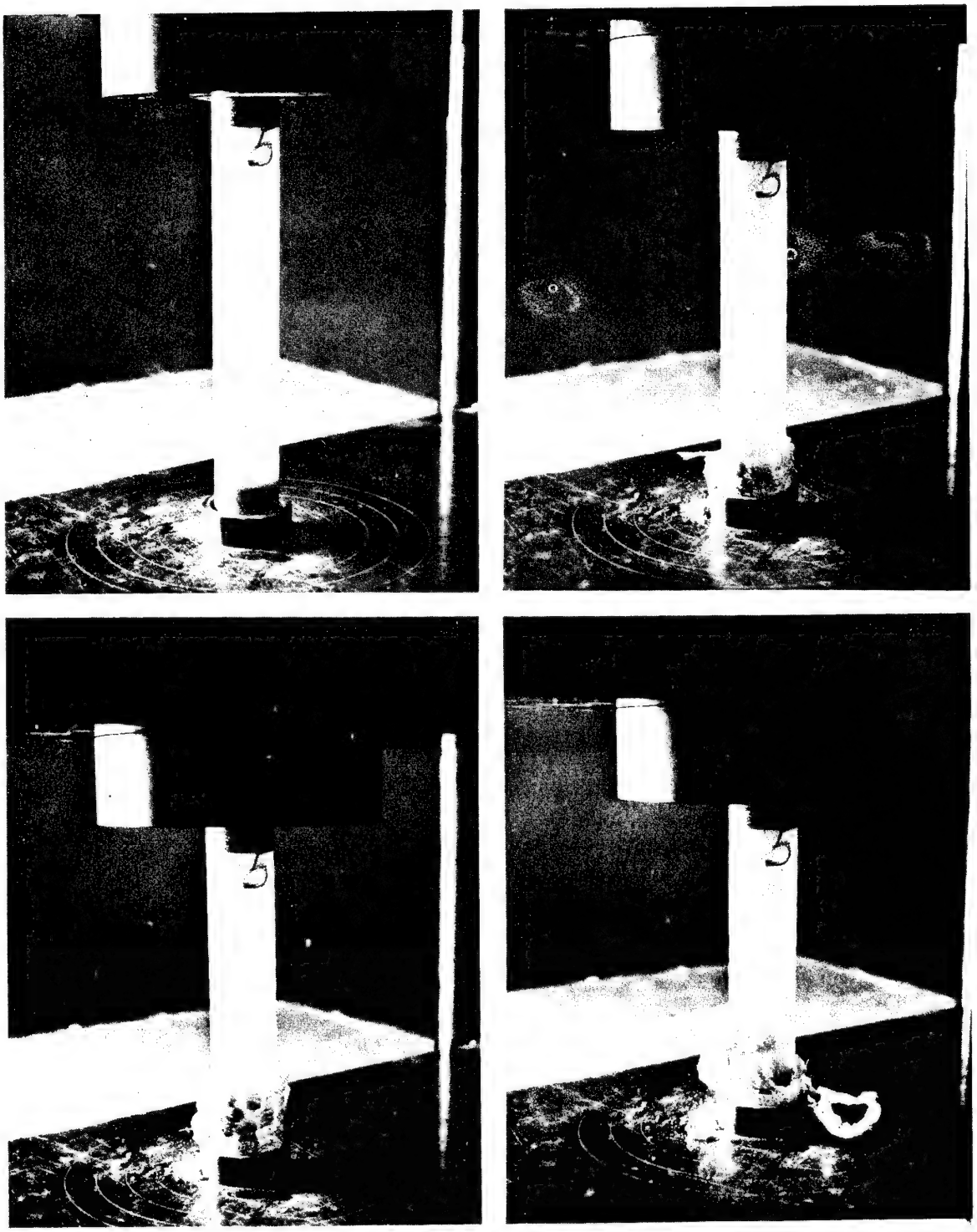

Figure 10. Typical 1.0 Inch I. D. 0.040 Wall Polyester Resin with 181 "E" Glass Fabric Fragmenting Tube Sequence

The results of the preliminary tube tests for the reinforced plastic laminated tubing are shown in Table II. Except for the four tubes noted, which were fabricated with epoxy resin systems, the tubing material was polyester resin with 143 or 181 fabric weave laminated mostly in three or four plies at 0.01 inch per ply. It will be noted that the tubing size was limited to a 1.0-inch diameter. Specific strengths as high as 21,800 ft-lb/lb were achieved with the polyester resin system. But the highest values were achieved with the higher strength epoxy resin system, which resulted in one value of 25,900 ft-lb/lb for a t/r of 0.741. Typical load displacement graphs are presented in Figure 11 for both unreinforced tubing which split or did not fragment and for the polyester resin system reinforced with 181 glass fabric. An outstanding characteristic of the polyester tube fragmenting load displacement graphs is the absence of an initial peak load; i.e., the GRP tubing demonstrated a load displacement graph shape which approached the ideal. The use of epoxy dies which were considerably lighter than the steel dies was limited because die choking was experienced due to the low bearing strength of the epoxy, and in some cases the dies fractured as shown in Figure 9.

TABLE II. PRELIMINARY TEST RESULTS FOR HAND-WRAPPED FRANGIBLE TUBES

t (in.)	D (in.)	r (in.)	Die Material	Fabric Weave	Average Force (lb)	F_f ksi	t/D	t/r	E_{sp} $\frac{\text{ft-lb}(10)^{-3}}{\text{lb}}$
0.030	1.060	0.054	Steel	143	1657	17.3	0.029	0.556	15.6
0.030	1.060	0.054	Steel	143	1100	11.3	0.029	0.556	11.3
0.040	1.080	0.054	Steel	143	1532	11.7	0.038	0.741	14.3
0.020	1.040	0.054	Steel	143	450	7.0	0.019	0.370	8.5
0.030	1.060	0.054	Steel	181	1300	13.4	0.029	0.556	17.0
0.030*	1.060	0.054	Steel	181	1100	11.3	0.029	0.556	14.2
0.030*	1.060	0.054	Steel	181	900	9.3	0.029	0.556	13.1
0.030	1.060	0.054	Plastic	181	1000	10.3	0.029	0.556	13.7
0.040	1.080	0.054	Steel	181	1900	14.5	0.038	0.741	18.1
0.040	1.080	0.054	Plastic	181	2260	17.3	0.038	0.741	21.8
0.040*	1.080	0.054	Steel	181	2200	16.8	0.038	0.741	21.3
0.040*	1.080	0.054	Plastic	181	2800	21.4	0.038	0.741	25.9
0.030	1.060	0.054	Steel	143	1550	16.0	0.029	0.556	19.0
0.030	1.060	0.054	Steel	181	1300	13.4	0.029	0.556	14.1
0.030	1.060	0.054	Steel	181	1450	15.0	0.029	0.556	16.2
0.030	1.060	0.054	Steel	181	1500	15.4	0.029	0.556	17.8
0.030	1.060	0.054	Plastic	181	1500	15.4	0.029	0.556	18.9
0.060	1.120	0.100	Steel	181	3750	18.8	0.054	0.600	19.6
0.030	1.060	0.100	Steel	181	750	7.7	0.029	0.300	8.9
0.030	1.060	0.075	Steel	181	950	9.79	0.029	0.400	10.8
0.040	1.080	0.075	Steel	181	1500	11.5	0.038	0.534	14.2
0.040	1.080	0.100	Steel	181	856	6.6	0.038	0.400	8.4
0.060	1.120	0.150	Steel	181	1650	8.3	0.054	0.400	11.6
0.060	1.120	0.200	Steel	181	1200	6.0	0.054	0.300	7.5
0.070	1.140	0.150	Steel	181	1800	7.7	0.061	0.466	6.8
0.070	1.140	0.200	Steel	181	1800	7.7	0.061	0.350	9.4
0.070	1.140	0.250	Steel	181	1051	4.5	0.061	0.280	4.0

*Epoxy Resin (All Other Polyester)

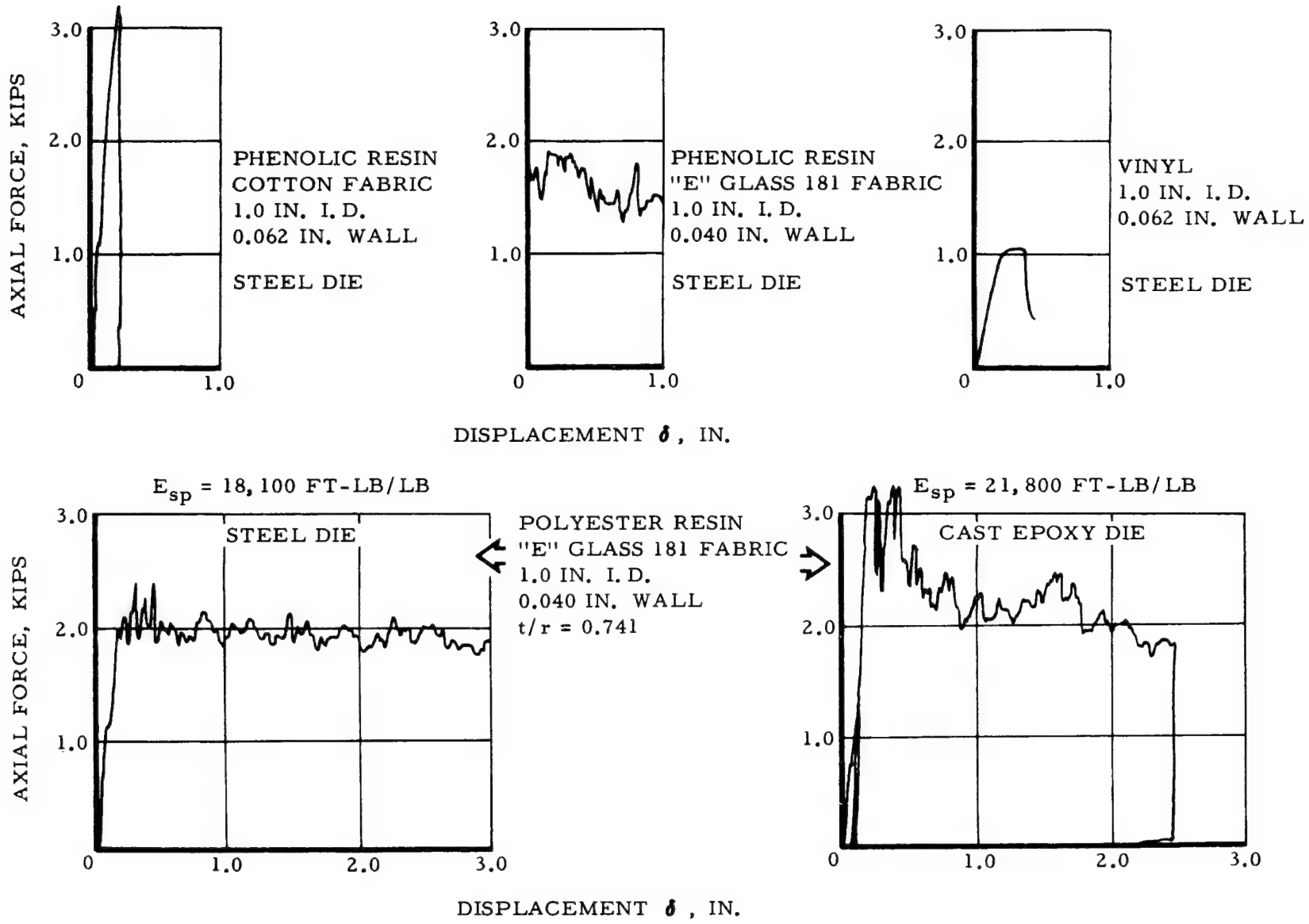

Figure 11. Typical Load Displacement Graphs for Various Plastic Tubes Fragmented over Steel and Plastic Dies as noted

Candidate Foam Element Materials. - A survey of the literature and of materials produced data that very few foams would qualify for the minimum specific energy of 10,000 ft-lb/lb requirement. The polyurethane foams would be useful as a fill material in a honeycomb composite system but the following rigid foams were the only types which indicated an acceptable specific strength:

1) A rigid pack-in-place polyurethane foam.
2) A rigid pack-in-place epoxy foam.
3) A rigid ceramic foam.
4) Glass macro-balloons and epoxy resin matrix.

The latter foam system is a combination of bonding agent, epoxy resin, loaded with glass macro-balloons. The macro-balloons are hollow glass spheres which in this case are not microspheres since they are 1/8 inch in diameter. This particular foam system was the most promising because it was developed as a buoyancy material for deep ocean submergence applications where high crushing strength and low density are the optimum requirements.

Preliminary Foam Element Crushing Tests. - A preliminary test was conducted on a ceramic foam (density of 12-lb/ft^3) which might crumble to powder after crushing and therefore be useful for the radio frequency transparency requirement after crushing. The estimated specific energy capability for this material was considered to be too low for use by itself, but characteristic load deformation curves and the crushed material condition might indicate its usefulness in combination with a honeycomb material. Figure 12 shows the test setup for a rectangular element shape. In all tests conducted the material first crumbled around the edges at the point of load application and load built up to a proportional limit which became rounded, then a sudden drop off of the load was experienced followed by continued gradual load reduction with stroke.

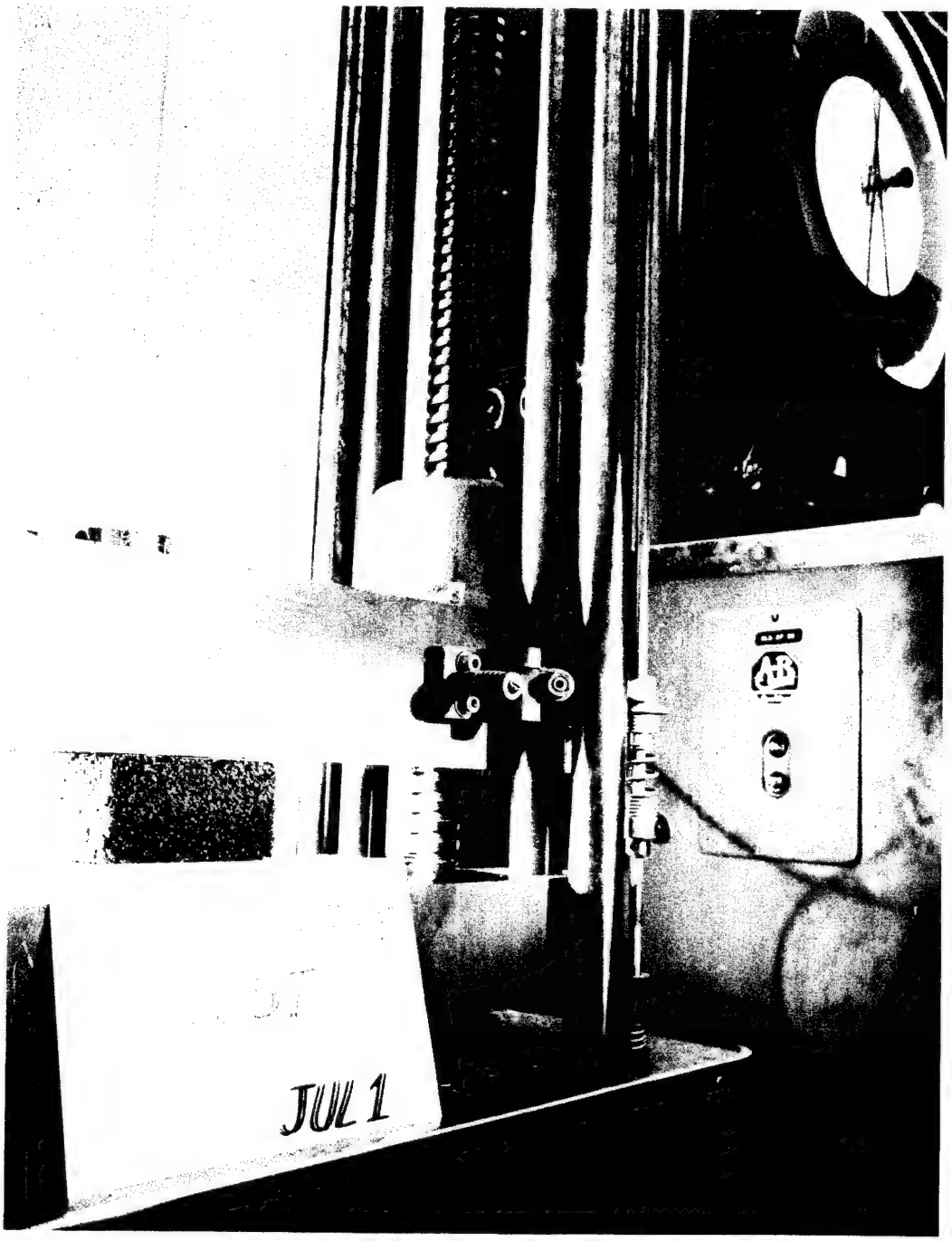

Figure 12. Ceramic Foam Test Set-up, Typical; Universal Testing Machine

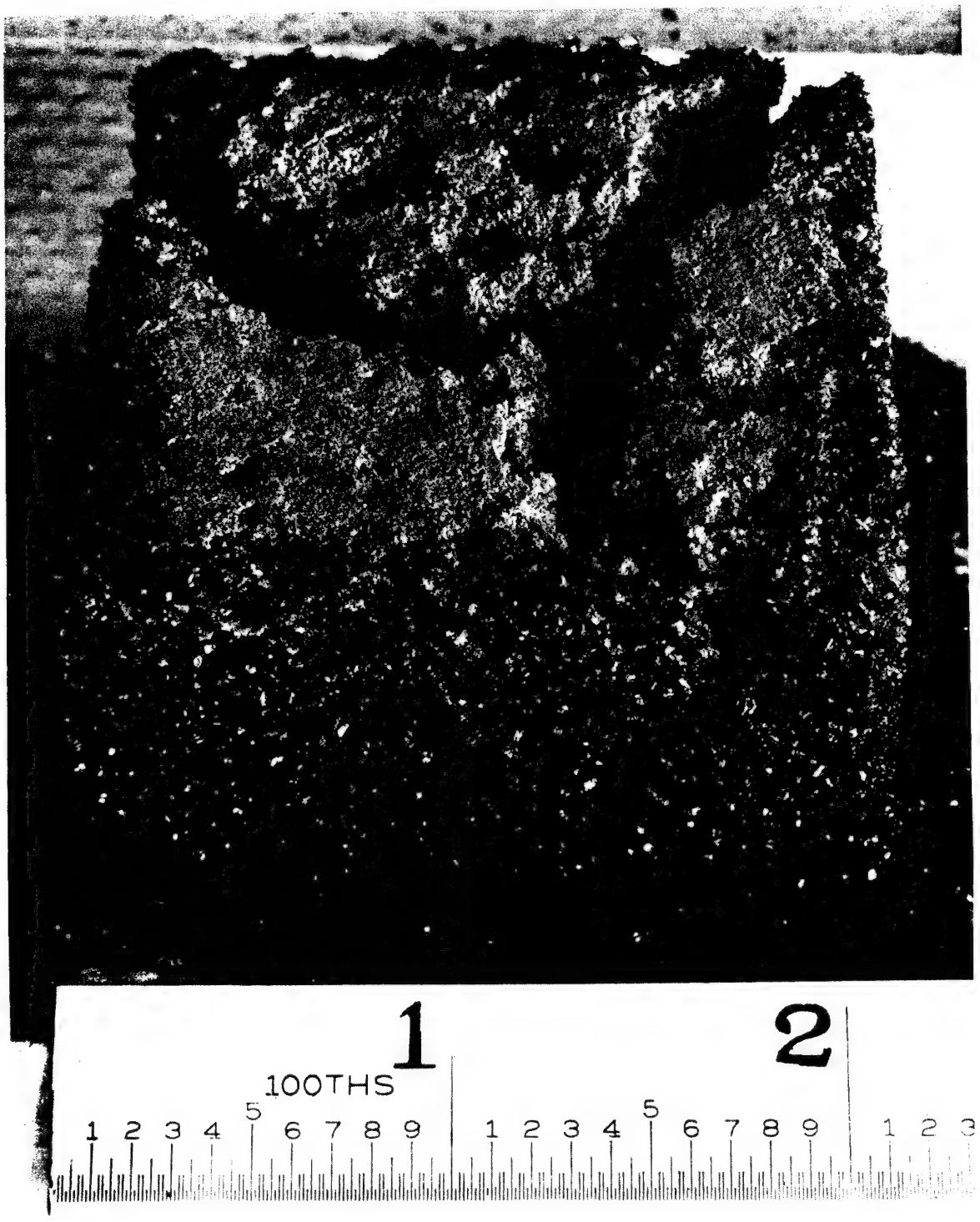

Figure 13. Ceramic Foam Specimen Showing First Signs of Failure

Figure 14. Ceramic Foam Specimens, Before and After Test

At the point of sudden load drop off a specimen such as that shown in Figure 13 was examined, and it was determined that the specimen had split. This splitting action varied with the size of the specimen. Figure 14 shows two sizes of specimens before and after testing indicating that the material does crush to a powder but that the specific energy and the shape of the load deformation curve was not acceptable for further evaluation.

Candidate Honeycomb Materials. - The results of previous investigators had indicated that the specific energy efficiency of honeycomb, particularly the aluminum alloy honeycomb material, was a function of the material yield strength and the ratio of core cell size to foil thickness. A survey of producers of honeycomb indicated that higher specific energy could be obtained by combining aluminum honeycomb with foam. By making comparisons of the compressive strengths of aluminum honeycomb with crushing strength, and by relating the results to the compressive strength density values of nylon phenolic honeycomb, three sizes of honeycomb in this material were selected for preliminary tests, as follows:

1) NP 3/16 -112-9.0; 9.0 lb/ft^3 density; estimated E_{sp} = 13,600 ft-lb/lb

2) NP 1/4 -21-8.0; 8.0 lb/ft^3 density; estimated E_{sp} = 11,700 ft-lb/lb

3) NP 3/8 -21-4.5; 4.5 lb/ft^3 density; estimated E_{sp} = 5,400 ft-lb/lb.

The estimates on the specific energy efficiency for the above three honeycomb elements were based on available compressive strength values which were divided by two to establish an assumed crushing strength.

Preliminary Honeycomb Element Crushing Tests. - Preliminary tests were conducted on honeycomb elements in the 12,000-lb capacity test machine. In some specimens a polyurethane foam was added to evaluate the characteristics of a composite. The results are tabulated in Table III.

TABLE III. PRELIMINARY TEST RESULTS, NYLON PHENOLIC HONEYCOMB

Cell Size (in.)	Specimen Size (in.)	Foam *Density (lb/ft^3)	F_f (psi)	E_{sp} $\frac{ft\text{-}lb(10)^{-3}}{lb}$
1/4	2-1/4x2x2	-	427	7.7
1/4	2x2x2	6	284	5.1
1/4	1x2x2	6	-	-
1/4	1x2x2	4	250	4.5
1/4	1x2x2	4	566	10.2
1/4	1x2x2	4	595	10.7
1/4	1-1/4x2x2	6	522	9.4
1/4	4x4x2	-	211	3.8
1/4	4x4x2	-	200	3.6
1/4	1x4x2	-	910	16.4
1/4	1x4x2	-	416	7.5
1/4	1/2x4x2	-	278	5.0
1/4	1x4x2	-	921	16.6
1/4	2x2x2	6	522	9.4
3/16	4x4x2	-	-	-
3/8	4x4x4	-	194	6.2
1/4	4x2x2	-	788	14.2
3/8	4x4x4	-	344	11.0
1/4	4x2x2	-	300	5.4
1/4	2x2x2	-	600	10.8
3/16	4x2x2	-	344	5.5
3/16	4x2x2	-	481	7.7
1/4	4x4x2	-	394	7.1

* Polyurethane Foam

Due to the limited capacity of the test machine, elements of the potentially most efficient cell size had to be tested in smaller sizes than were considered to provide useful information, because of the influence of the boundary cell failure on the total cell failure pattern. The effect of filling the honeycomb with foam was to improve the efficiency sufficiently to meet minimum 10,000 ft-lb/lb strength requirements. It was concluded that all future specimens should be larger to provide more consistent and more meaningful results. This decision would require the use of a larger test machine.. Figure 15 shows typical load deformation plots for these preliminary honeycomb tests for unfilled and foam-filled honeycomb. The foam-filled honeycomb had a definite initial peak and a final buildup at the end of the stroke. The honeycomb by itself showed no initial peak as was experienced in the aluminum honeycomb tests.

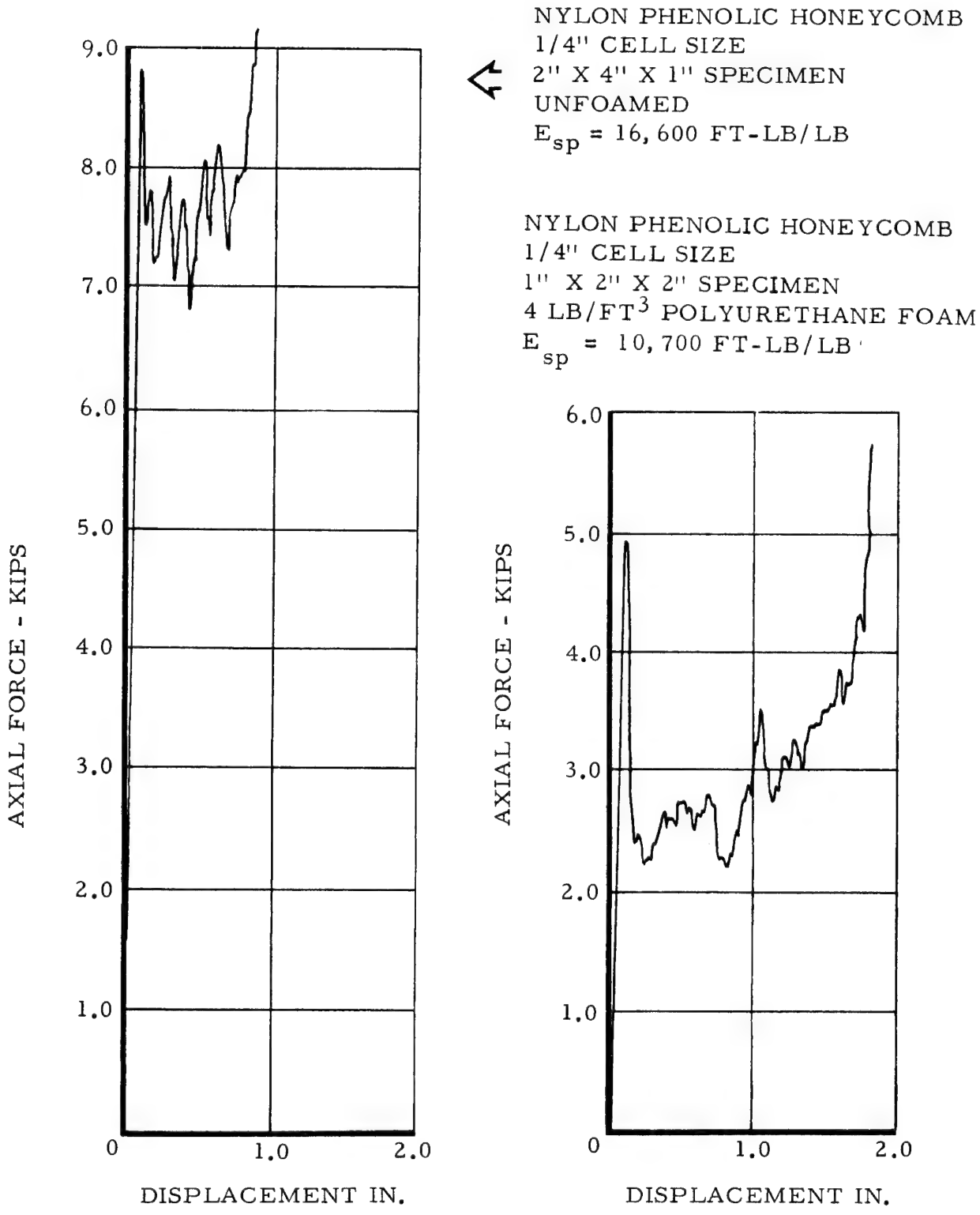

Figure 15. Comparisons of Nylon Phenolic Honeycomb 1/4 in. Cell Size With and Without 4 lb/cu ft Polyurethane Foam Filling

SPECIMEN FABRICATION

Plastic Tube Fabrication. - The fiberglass-reinforced polyester and epoxy tubes used throughout the test program were fabricated from the following commercially impregnated glass fabric:

MILITARY SPEC	RESIN TYPE	FABRIC STYLE
MIL-R-9300	EPOXY	143
MIL-R-9300	EPOXY	181
MIL-R-7575	POLYESTER	181
MIL-R-7575	POLYESTER	143

The materials listed above were selected for tubular test specimen construction because past experience indicated they were of high and consistent quality. Tubes were fabricated from these materials by two basic procedures -- hand layup and machine wrap.

Hand Layup. - The hand layup technique consists of cutting a 10-inch-wide strip of pre-impregnated glass fabric (pre-preg) in sufficient length to allow for the required number of tube plies. The 10-inch width may be taken in either the warp or fill direction of the pre-preg, depending upon the desired fiber orientation in the resultant tube. The 10-inch edge of the strip of pre-preg is pressed firmly against the surface of a 1.0-inch diameter steel mandrel which has previously been coated with release agent. The pre-preg strip is carefully wrapped around the mandrel the desired number of times to obtain the required tube wall thickness. Care must be employed during the wrapping to assure a smooth, tight wrap free of wrinkles and entrapped air. After the desired number of plies have been wound on the mandrel, the pre-preg strip is cut to a length which will just allow the bottom edge to overlap the first ply edge by 1/2 inch. One end of the tube is built up by wrapping an additional ten plies of 1/2 inch wide pre-preg on it; this build-up will serve as a bearing

surface reinforcement during the stripping operation. The pre-preg layup is then spiral wrapped with a 1-inch-wide polyvinyl alcohol tape in such a manner as to overlap one half of the tape width on each successive turn. The spiral wrapping procedure is continued the whole length of the mandrel and then repeated in the same overlapping fashion back along the tube length in the reverse direction. This results in a double overlapping layer of plastic film covering the pre-preg layup. The plastic film over-wrap serves as the method of applying pressure to the plastic layup during the heat curing operation; the film shrinks under heat and the attendant hoop tension pressure is applied to the tube during cure. The mandrels are then placed in an air circulating oven and cured according to the following schedule:

RESIN	CURE CYCLE
Polyester	3 hours at 275°F
Epoxy	4 hours at 325°F

After the tube has been cured, the film over-wrap is removed and the tube stripped from the mandrel. The tube stripping is accomplished by means of a stripping block, a mandrel punch, and a stripping sleeve. The stripping block is a thick, flat piece of metal with a 1.00-inch-diameter hole which slips over the mandrel and bears against the tube at the builtup end. The mandrel punch is a piece of rod stock having a diameter slightly less than the mandrel itself. This punch is placed on the end of the mandrel with the stripping block in position. This assembly, the stripping block, mandrel, and mandrel punch are placed on the stripping sleeve, which is simply a 1-1/2-inch I.D. pipe 14 inches long. The tube is extracted from the mandrel by pressing the mandrel into the stripping sleeve with the mandrel punch. The stripping block is supported by the stripping sleeve and bears against the tube, thus removing the tubular specimen from the mandrel. The tubes are then trimmed and the ends squared off by means of a diamond cut-off wheel and submitted for testing.

Machine Wrap. - Additional tubes were fabricated by the use of a tape wrapping machine. As illustrated in Figures 16 and 17, this machine is normally used to wrap thick section plastic parts used for high temperature environments, but is equally capable of wrapping thin wall tubes. The procedure for wrapping these tubes is as follows:

1) Place the mandrel coated with parting agent in the rotary chuck.
2) Press the leading edge of the pre-preg strip against the mandrel surface.
3) Close the pressure rollers against the mandrel and apply 3000 lb pressure.
4) Start the machine and wind at 20 rpm. Wind the desired number of plies using moderate tension.
5) Stop the machine and cut the pre-preg so that it overlaps the first edge of the material strip by 1/2 inch.
6) Restart the machine and run for two minutes maintaining 3000 lb pressure on the pressure rollers.
7) Stop the machine and release pressure from the pressure rollers.
8) Wind ten additional plies of 1/2-inch-wide pre-preg strips on one end of the tube.
9) Spiral wrap two layers of polyvinyl alcohol tape on the layup in a manner similar to that described for the hand layup tubes. Maintain moderate tension on the tape during winding operation.
10) Stop the machine, remove the mandrel from the chuck, and cure, trim, and finish in the same manner as the hand layup tubes.

Miscellaneous Specimen Preparation. - In addition to fiberglass-reinforced plastic tubes, the following types of specimens were also prepared and tested during the program: purchased tubing (thermosetting and thermoplastic), ceramic foam, epoxy syntactic foam, fiberglass reinforced phenolic honeycomb, and honeycomb stabilized with syntactic foam.

Tubes. - These plastic tubes were purchased with a nominal I.D. of 1.0 inch and represent the various types of commercially available tubing.

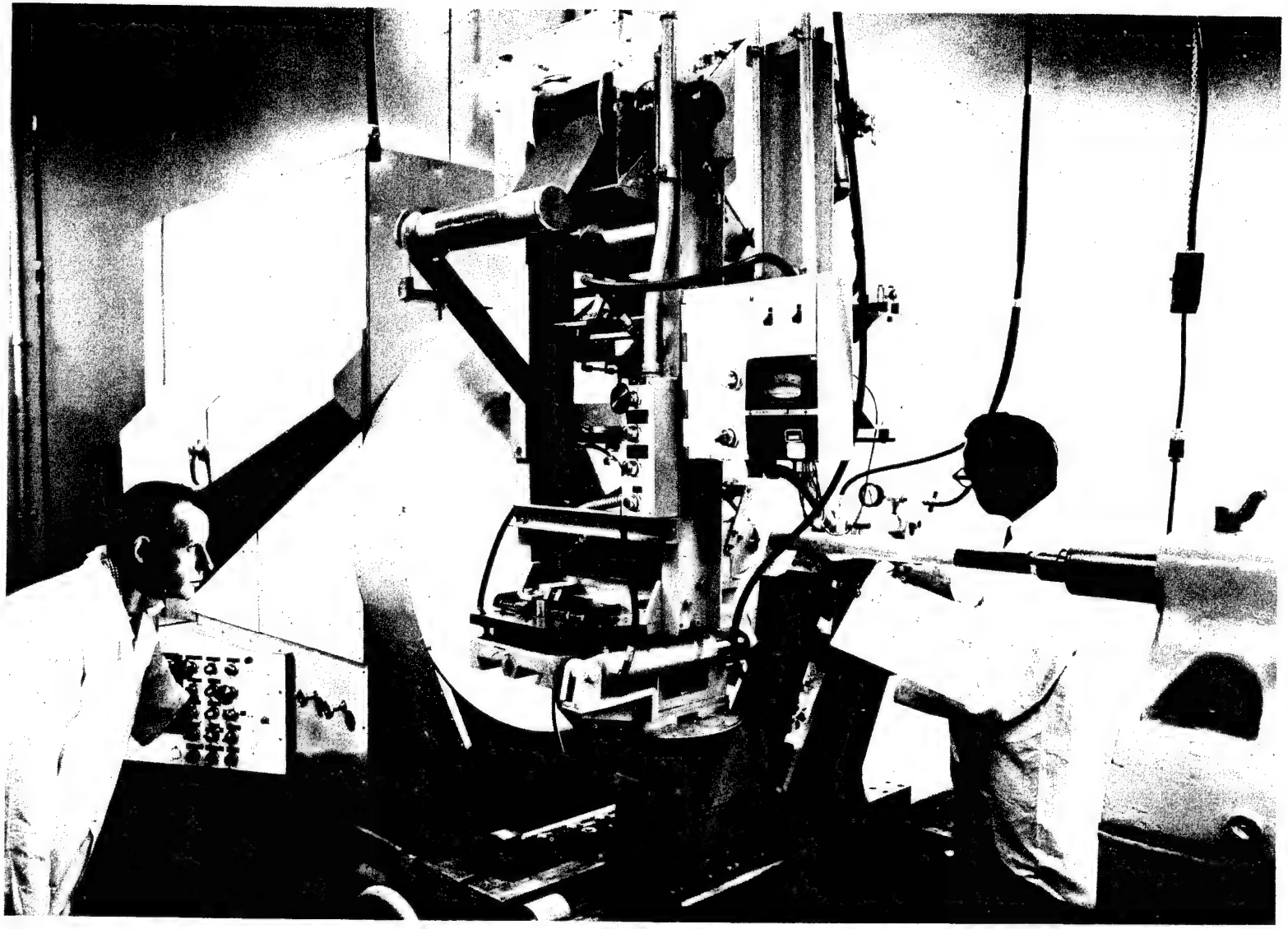

Figure 16. Tape Applicator for Wrapping Plastic Products

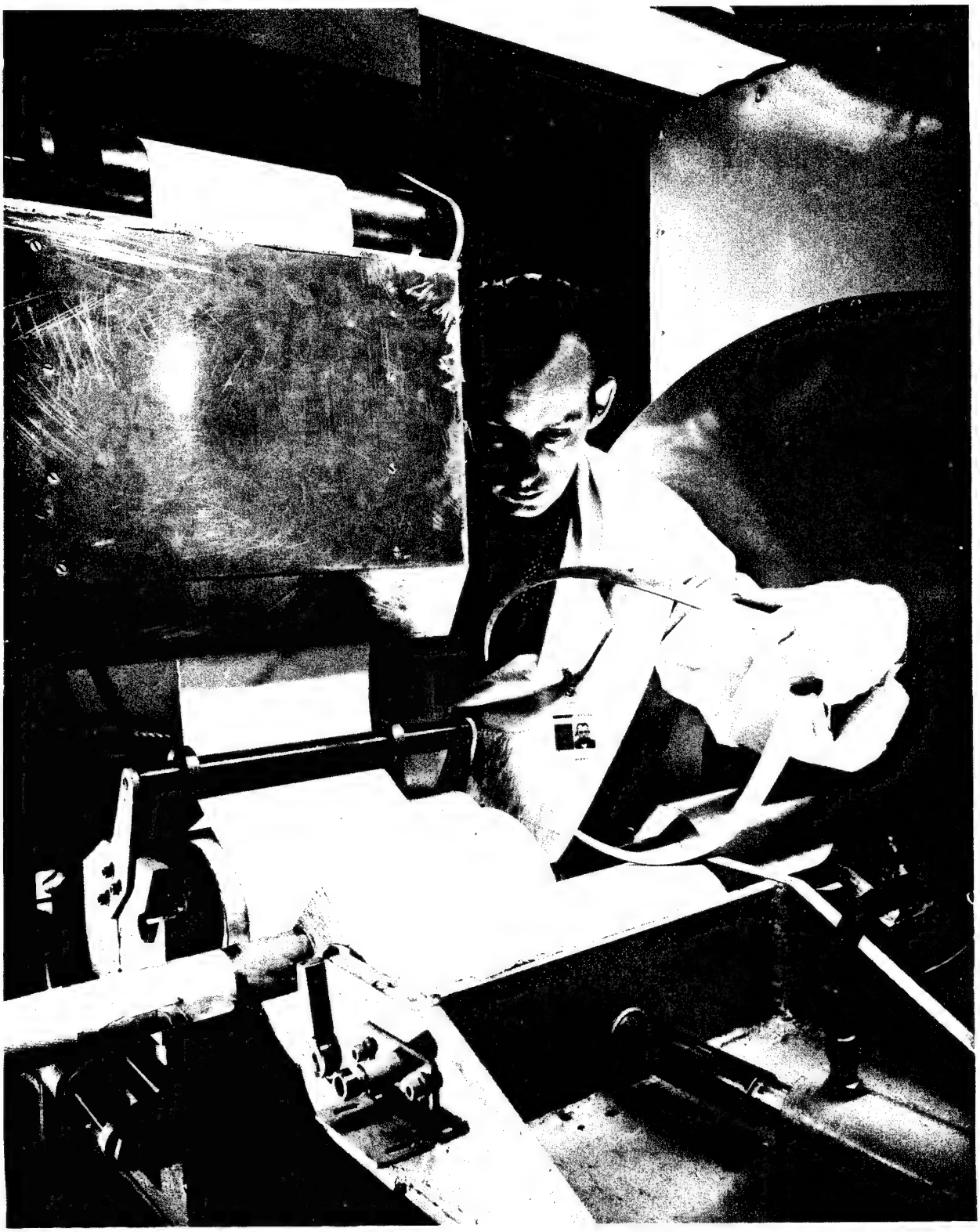

Figure 17. Rollers Provide Controlled Hydraulic Pressure for Debulking Plastic Material

The only specimen preparation required was to cut the tubing in column-stable lengths. These specimens were tested using the same dies used to test the fabricated tubing specimens.

Ceramic Foam. - The ceramic foam was purchased in the form of a rectangular block. Test specimens were cut from this block by means of a diamond cut-off wheel, employing extreme care to machine opposite specimen faces parallel.

Epoxy Syntatic Foam. - Syntactic foam used to prepare test specimens was formulated in three different densities by adjustment of the amounts of the components blended. The components used to formulate the foam were an epoxy resin matrix and small, hollow glass macro-balloons. The glass macro-balloons are suspended in a one part epoxy-based matrix; the glass macro-balloons are hollow, thin-walled resin spheres ranging in diameter from 0.130-0.180 inch and having a bulk density of 15.6 lb/ft^3. The epoxy resin system requires a heat cure of 5 hours at 200° F followed by 2 hours at 300° F. Test specimens were prepared by two different methods: 1) the specimens were cast to net dimensions and, 2) the specimens were cut from a large pre-cast block to net dimensions. Specimens cast to net dimensions had undamaged plastic spheres throughout the sample while specimens cut from the pre-cast block had fractured spheres on the machined faces. Both types of specimens were tested in the program.

Fiberglass Reinforced Phenolic Honeycomb. - Honeycomb specimens were prepared by sawing standard dimension specimens from a large honeycomb block. Specimens were prepared and tested in three different cell sizes - 3/16, 1/4, and 3/8 inch.

Honeycomb-Syntactic Foam. - The composite syntactic foam-honeycomb specimens were prepared by casting the foam resin in the 3/8 inch cell size honeycomb specimens. Composite specimens were prepared using two

different density foam formulations. The foam was heated to lower the viscosity and allow for pouring of the lower density formulation into the honeycomb cells. The specimens were then cured according to the manufacturer's recommended procedure.

Fabrication of Plastic Dies. - Fabrication of the epoxy plastic dies was accomplished by using the metal die as the pattern master according to the following procedure:

a) Coat the metal die with release agent. Also coat the inner surfaces of a 6 oz dixie cup with the parting agent.

b) Position the die in the center of the dixie cup and fill to a level covering the die with a silicone elastomer casting compound.

c) Allow to cure and separate metal die from silicone elastomer pattern.

d) Coat the molding surface of the RTV #11 pattern with release agent #225 and fill cavity with Casting Epoxy.

e) Allow epoxy to cure and remove the cast die from the silicone elastomer mold.

MECHANICAL DEFORMATION TESTS

Test Equipment. - The majority of the mechanical crushing tests and all of the tube fragmenting tests were conducted on the 12,000-lb maximum-capacity universal test machine (see photograph of figure 12). This machine is equipped with a ram deflectometer which measures head travel over 10.0 inches of gage length. The machine is equipped with an X-Y recorder for graphically recording load-deformation curves. This machine is also equipped with a load pacer device, a load cycling mechanism, and constant head travel control from 0- to 20-inches per minute.

A universal testing machine similar to the one described but with a 120,000-lb maximum capacity was used for some of the large load foam and honeycomb tests.

Nylon Phenolic Honeycomb Tests. - A typical nylon phenolic honeycomb specimen, 4 x 4 x 2, is shown in Figure 18 before and after crushing tests. Three specimens of 3/8-inch cell size, and three specimens of 1/4-inch cell size, and three specimens of 3/16-inch cell size were tested by crushing in the 2-inch depth direction until the load buildup at the end of the stroke became very steep, indicating the limit of usable stroke. Each specimen was weighed and this weight was used in conjunction with the area under the load stroke curve to determine the specific energy absorbing efficiency. Table IV shows the test results for these specimens. The specific energy shown calculated contains the usable stroke which is, therefore, a realistic efficiency evaluation. A higher efficiency could have been calculated than that shown if the actual stroke was used in the calculations. The results are consistent and bear out the preliminary estimated efficiencies except in the case of the 3/16-inch cell size which is the only size which qualifies for the 10,000 ft-lb/lb limitation. In this cell size the estimated efficiency was not based on usable stroke limitations and therefore would

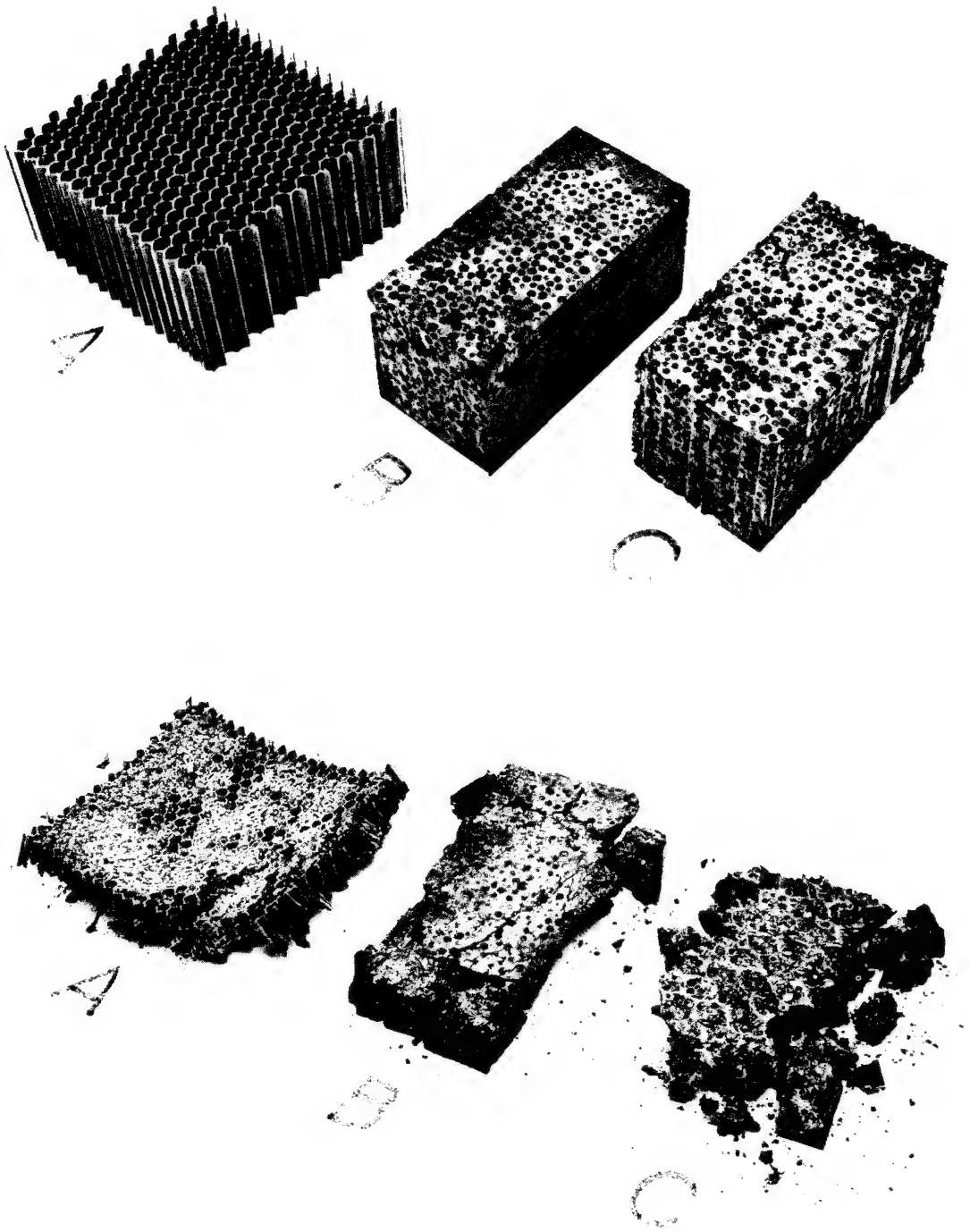

Figure 18. Test Specimens of (A) Nylon Phenolic Honeycomb (B) Syntactic Foam Filled with Glass Micro Balloons (C) A Combination of Specimens (A) and (B), Before and After Testing

TABLE IV. TEST RESULTS FROM CRUSHING SPECIMENS OF HONEYCOMB, FOAM, AND FOAM-FILLED HONEYCOMB

Type of Specimen	Cell Size (in.)	Density (lb/ft^3)	Usable Stroke (%)	F_{cc} (psi)	E_{sp} $\frac{ft\text{-}lb(10)^{-3}}{lb}$
Nylon Phenolic Honeycomb	3/8	4.5	50	225	3.60
	3/8	4.5	50	200	3.20
	3/8	4.5	80	138	3.53
	1/4	8.0	75	688	9.30
	1/4	8.0	80	625	9.00
	1/4	8.0	75	625	8.45
	3/16	9.0	80	1125	14.4
	3/16	9.0	80	1094	14.0
	3/16	9.0	80	1125	14.4
Nylon Phenolic Honeycomb filled with Syntactic Foam and Micro-Balloons	3/8	28.9	55	1941	5.33
	3/8	27.8	60	1915	5.95
	3/8	31.1	60	1970	5.47
	3/8	29.0	60	1760	5.25
Syntactic Foam and Micro-Balloons	N/A	31.6	70	1650	5.26
		31.4	70	1650	5.30
		32.0	65	2030	5.94
		34.2	68	2350	6.73
		34.8	65	3050	8.20
		34.8	75	2540	7.88
		27.4	70	888	3.26
		27.4	70	1015	3.74
		26.8	70	888	3.34

have been a lower value. The actual difference can be attributed to the fact that plastic honeycomb material has no initial peak load compressive strength, therefore the compressive strength is also the crushing strength. Tests were also conducted on four 3/8-inch cell size nylon phenolic honeycomb specimens of 2 x 4 x 2-inch size filled with syntactic foam of approximately 32 lb/ft^3 density. The results in Table IV show a significant efficiency improvement over the unfilled 3/8-inch honeycomb but the actual values were half the minimum required specific energy.

Syntactic Foam Tests. - Nine specimens of syntactic foam material in groupings of three each of 30, 32 and 35 lb/ft^3 density were tested in the 120,000-lb capacity test machine. The specimens were similar to the one shown before and after test in Figure 18. It was indicated that the specific energy efficiency improved with increasing density and was approaching the minimum acceptable value with a density of 35 lb/ft^3.

Discussion of Honeycomb and Foam Results. - A typical load deformation graph for syntactic foam of approximately 35-lb/ft^3 density is shown in Figure 19. This material peaks sharply at the beginning of the stroke and then has a two-step load dropoff to a fairly steady load with increasing deformation until the load builds up again rapidly at the end of the stroke. The usable stroke is limited to 70% of the specimen depth. The specific energy absorption capability of this material was much below the minimum required value and the shape of the load deformation curve was not close to the ideal. Figure 20 presents typical load deformation graphs for syntactic foam-filled nylon phenolic honeycomb and for the unfilled honeycomb. The syntactic foam-filled honeycomb had a load deformation plot with a slight peak at the beginning and end of the stroke, otherwise it approached an ideal shape; however the energy absorption efficiency was not close to the minimum value required. The unfilled nylon phenolic honeycomb load deformation plot as shown was an ideal shape. The 3/16-inch cell size shown

in Figure 20 was the cell size which had a specific energy efficiency of 14,400 ft-lb/lb and therefore represents a considerable improvement over aluminum alloy honeycomb as an energy absorption structural element. All crushed material from these element tests was collected and prepared for radio frequency transparency testing.

Fragmenting Tube Tests.- A evaluation of the results of the preliminary tube tests indicated that 143 fabric, which is highly directional in strength, could not be used because the tubes split rather than commencing to fragment. The 181 bi-directional fabric furnished good fragmenting results in some cases, especially with the higher strength epoxy resin system; consequently the test program was limited to 1.0-inch-diameter tubes with 181 fabric laminates with an epoxy resin system fabricated by a hand layup process. The results of the test program are tabulated in Table V. All testing was conducted with steel dies at a 1.0-inch-per-minute loading rate. There were more than 50% of the tubes tested which qualified for the 10,000 ft-lb/lb specific energy restriction with one tube fragmenting at a specific energy level of 25,200 ft-lb/lb. This particular tube was made with four plies and had a tube to die t/r of 0.682. This ratio was lower than the ratio which was used in the preliminary tests which also resulted in a similar energy value. An examination of these results indicated that scatter between tubes of similar dimension was significant. An investigation of the fragmented tubes indicated that a different fabrication process should improve the repeatibility of results among similar specimens and scatter could be reduced. It was also concluded that the splitting in the 143 tubing may also be attributed to the hand layup fabrication process. As a result of the indicated scatter in the tests shown in Table V, additional testing was planned using a new method of fabrication for the tube specimens. The new series of tubes were fabricated on the tape wrapping applicator which is illustrated and described in the specimen fabrication section of this report. One feature of the applicator is that the fabricator can apply a 3000-lb pressure to the

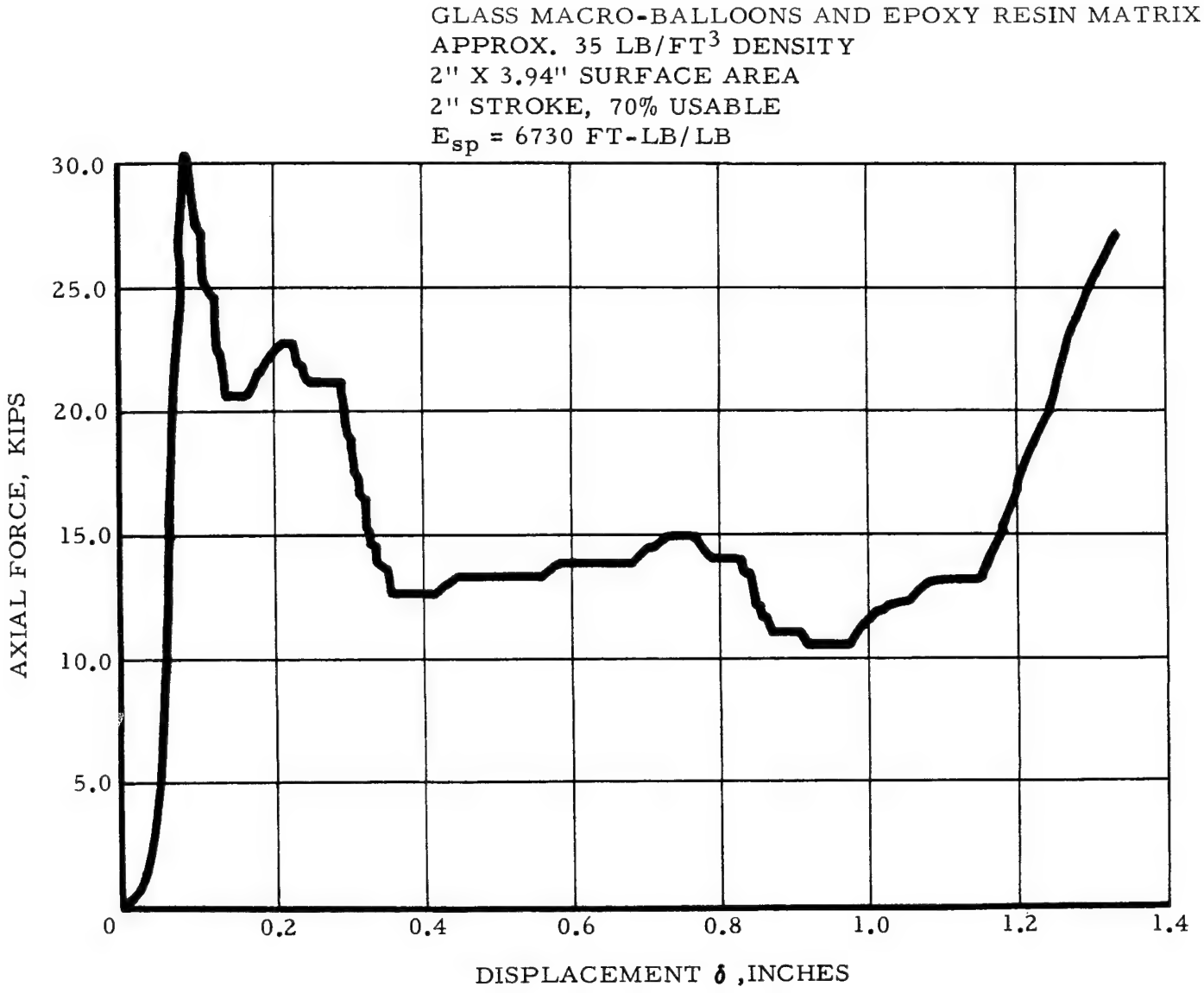

Figure 19. Typical Syntactic Foam Radio Frequency Transparent Load Displacement Graph for Specimen Type "B" Shown in Figure 18

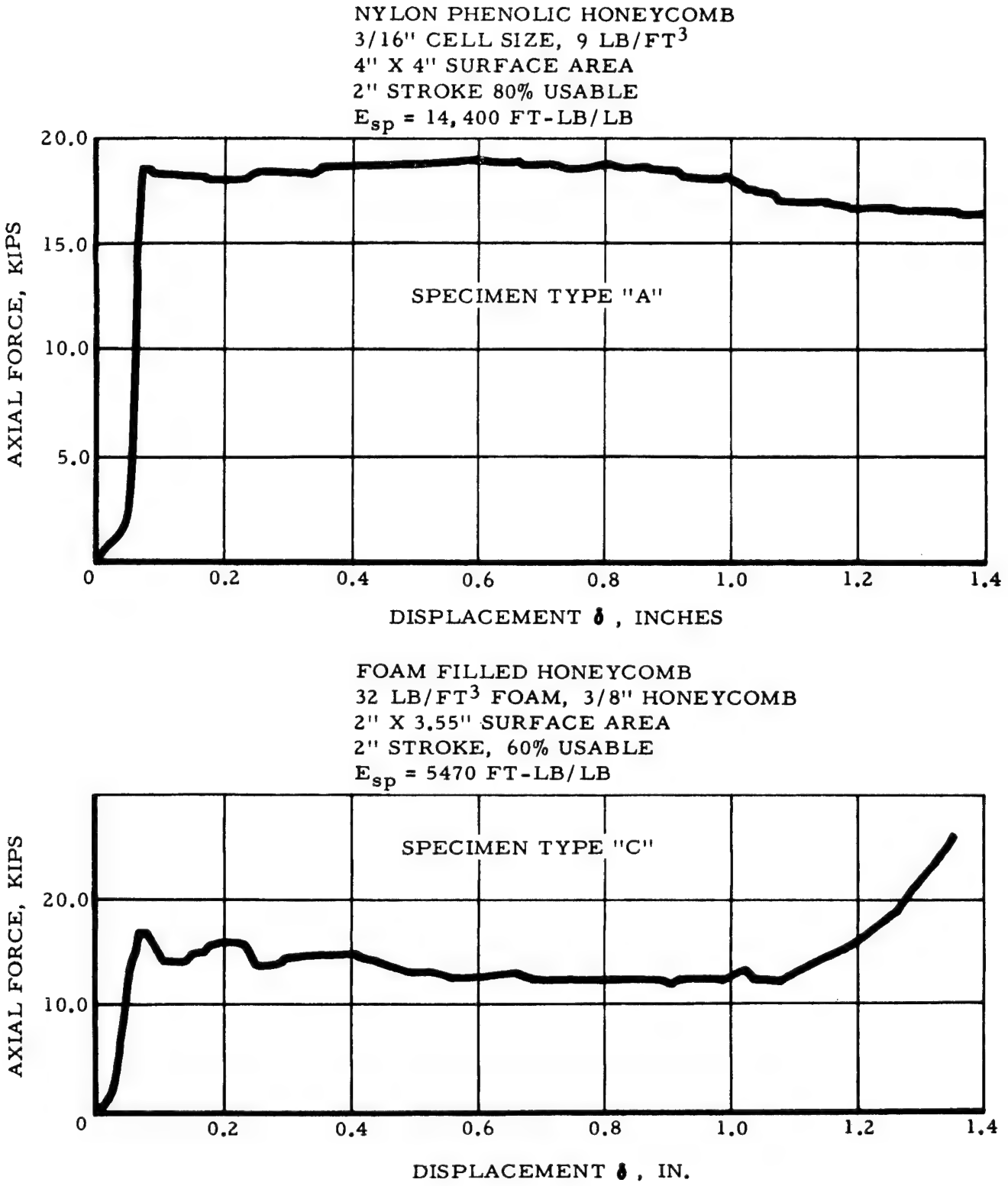

Figure 20. Typical Radio Frequency Transparent/Nylon Phenolic Honeycomb Load Displacement Graphs for Specimen Types "A" and "C" Shown in Figure 18

TABLE V. TEST RESULTS FROM FRAGMENTING HAND-WRAPPED TUBES OF EPOXY RESIN WITH 181E GLASS FABRIC

No. of Plies	r (in.)	t/r	P_{ave} (lb)	F_f (psi)	$\frac{E_{sp}}{f\ t\text{-}lb(10)^{-3}/lb}$	REMARKS
4	0.050	1.038	--	--	--	Die, loaded; tube buckled
4	0.075	0.605	2250	15,800	19.8	Tube began splitting at end of stroke
4	0.075	0.605	2300	16,150	17.9	
4	0.100	0.505	2500	15,750	11.1	Die loading
4	0.100	0.467	2200	15,000	20.3	Die loading
4	0.100	0.467	2300	15,700	14.3	Fragmenting
4	0.100	0.482	2000	13,200	18.9	Fragmenting
4	0.100	0.482	1800	11,900	15.2	Fragmenting
4	0.150	0.315	1200	8,090	11.0	Fragmenting
4	0.150	0.312	--	--	--	Tube split and fractured
4	0.150	0.330	900	5,800	8.0	Fragmenting
4	0.150	0.330	950	6,110	8.2	Fragmenting
4	0.200	0.262	--	--	--	Tube split and fractured
4	0.200	0.262	--	--	--	Tube split and fractured
4	0.200	0.236	500	3,380	4.3	Fragmenting
4	0.200	0.236	600	--	--	Tube split
4	0.200	0.236	650	4,400	6.2	Fragmenting
4	0.250	0.210	--	--	--	Tube split
4	0.075	0.682	3000	18,690	25.2	Fragmenting
3	0.050	0.645	960	9,500	14.3	Fragmenting
3	0.050	0.645	--	--	--	Tube fractured
3	0.050	0.681	1100	10,290	13.7	Some die loading
3	0.050	0.681	1640	15,300	19.2	Tube fragmented at upper end (some)

TABLE V. (Continued)

No. of Plies	r (in.)	t/r	P_{ave} (lb)	F_f (psi)	$\frac{E_{sp}}{\frac{ft\text{-}lb(10)^{-3}}{lb}}$	REMARKS
3	0.050	0.715	1300	11,600	15.6	Fragmenting
3	0.050	0.715	1480	13,200	18.7	Tube fractured at upper end, at end of stroke
3	0.075	0.468	900	8,160	11.1	Fragmenting
3	0.075	0.968	920	8,340	12.1	Tube fractured at end of of stroke
3	0.075	0.471	1540	13,900	16.9	Fragmenting
3	0.075	0.471	1300	11,700	14.9	Fragmenting
3	0.075	0.475	1120	10,000	14.1	Fragmenting
3	0.075	0.475	1000	8,950	13.5	Fragmenting
3	0.100	0.346	880	8,100	11.1	Fragmenting
3	0.100	0.346	1000	9,210	11.7	Fragmenting
3	0.100	0.361	960	8,470	12.3	Fragmenting
3	0.100	0.361	960	8,470	11.7	Fragmenting
3	0.100	0.370	840	7,240	10.4	Fragmenting
3	0.100	0.370	800	6,900	9.9	Fragmenting
3	0.150	0.230	400	3,700	5.3	Fragmenting
3	0.150	0.230	500	4,620	5.9	Fragmenting
3	0.150	0.235	420	3,790	5.1	Fragmenting
3	0.150	0.235	420	3,790	5.0	Fragmenting
3	0.150	0.239	420	3,640	5.2	Fragmenting
3	0.150	0.239	400	3,470	--	Final weight not recorded
3	0.075	0.680	1000	9,360	12.0	Fragmenting
3	0.075	0.461	1180	10,880	12.4	Fragmenting
3	0.050	0.461	1260	11,600	14.7	Fragmenting

mandrel to remove all entrapped air and to ensure a positive bond between laminate layers. The new series of tubes were also 1.0-inch diameter fabricated with an epoxy resin system and with fabric weaves of 181 fabric and of 143 fabric oriented in the hoop direction for some tubes and in the longitudinal direction for other specimens. A theory that the primary contribution to the fragmenting efficiency of tubing is in the breaking of the longitudinal fingers after the tube splits into multiple fingers was borne out by tests of the 143 fabric specimens as shown in Table VI. Splitting was again encountered in the longitudinally oriented 143 fabric specimens, but those specimens which did fragment provided the highest specific energy values for longitudinally oriented 143 fabric, and the lowest values for the hoop oriented fabrics. The highest value of the program was obtained in these tests with 28,400 ft-lb/lb specific energy for a four-ply longitudinally orientated 143 fabric with a t/r of 0.330. The 181 fabric tubes showed repeatability in specific energy for similar geometry and the highest value with this fabric weave was 23,800 ft-lb/lb for a t/r of 0.565.

The actual fragmented tube debris which was obtained for the differently orientated fabrics and different weaves varied with the fabrics and the weave orientation as shown in Figure 21. A typical load deformation plot for a 181 fabric weave epoxy resin system tube is shown in Figure 22. There is no initial peaking of the curve at the beginning of the stroke and the magnitude of the load oscillation during the stroke is much smaller than was obtained in the fragmenting tests of aluminum alloy tube. Several additional tubes in this extra series were tested at 20.0 inches per minute as compared with the program test rate of 1.0 inch per minute. Figure 23 illustrates the fragmented tube after the high loading rate run. The actual shape of the load deformation curve was rectangular with no initial peaking and with no significant oscillation of the load level with stroke as was recorded in the low-speed run. The specific energy obtained for the high-speed run was slightly higher than that obtained for a similar specimen run at 1.0 inches per minute.

TABLE VI. TEST RESULTS FROM TAPE-WRAPPED TUBES OF EPOXY RESIN WITH 181 AND 143 E GLASS FABRIC

Type of Weave	No. of Plies	r(in)	t/r	P_{ave} (lb)	F_f (psi)	$E_{sp} \times 10^{-3}$ (ft-lb/lb)	Remarks
181	3	0.050	0.510	750	9380	10.9	Fragmented
181	3	0.050	0.578	800	8820	10.6	Fragmented
181	3	0.050	0.502	-	-	-	Upper end failed
181	4	0.050	0.748	1275	11,600	13.4	Fragmented
181	4	0.050	0.788	1350	11,480	13.1	Fragmented
181	4	0.075	0.520	1400	11,420	13.8	Fragmented
181	6	0.100	0.584	3600	19,650	21.8	Fragmented
181	6	0.100	0.565	3400	19,150	23.8	Fragmented
181	6	0.150	0.400	-	-	-	Tube buckled, 4 plies longitudinal
143	4	0.075	0.518	-	-	-	Tube split, 4 plies hoop direction
143	4	0.075	0.396	-	-	-	Upper end failed
143	4	0.100	0.330	2600	25,000	28.4	4 plies longitudinal
143	4	0.100	0.335	2200	20,900	21.6	4 plies longitudinal
143	4	0.100	0.374	1300	11,050	12.3	4 plies hoop direction
143	4	0.100	0.312	1100	10,100	9.9	4 plies hoop direction
143	4	0.100	0.412	1800	13,920	12.3	3 ply longitudinal 1 ply hoop direction
143	4	0.100	0.468	2000	13,630	17.0	3 ply longitudinal 1 ply hoop direction
143	4	0.075	0.437	2700	19,650	24.0	3 ply longitudinal 1 ply hoop direction
143	4	0.100	0.391	2900	23,600	26.8	4 ply longitudinal
143	4	0.100	0.447	3100	26,300	26.3	4 ply longitudinal
143	4	0.100	0.391	-	-	-	Tube split
143	5	0.100	0.522	-	-	-	Tube split
143	5	0.150	0.338	-	-	-	Tube split
143	5	0.150	0.352	-	-	-	Tube split
143	6	0.150	0.404	-	-	-	Tube split
143	6	0.200	0.302	-	-	-	Tube split
143	6	0.100	0.575	4600	25,600	29.4	4 ply longitudinal

4 PLIES WITH STRENGTH ORIENTED IN LONGITUDINAL DIRECTION

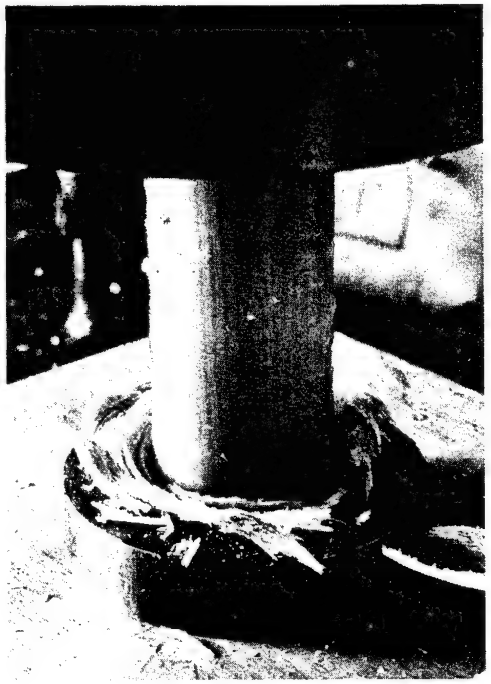

4 PLIES WITH STRENGTH ORIENTED IN HOOP DIRECTION

3 PLIES WITH STRENGTH ORIENTED IN LONGITUDINAL DIRECTION, 1 PLY WITH STRENGTH ORIENTED IN HOOP DIRECTION

Figure 21. Effect of Ply Orientation on Specimens Constructed of 143 "E" Glass Fabric and Epoxy Resin, Fabricated on NV Tape Applicator

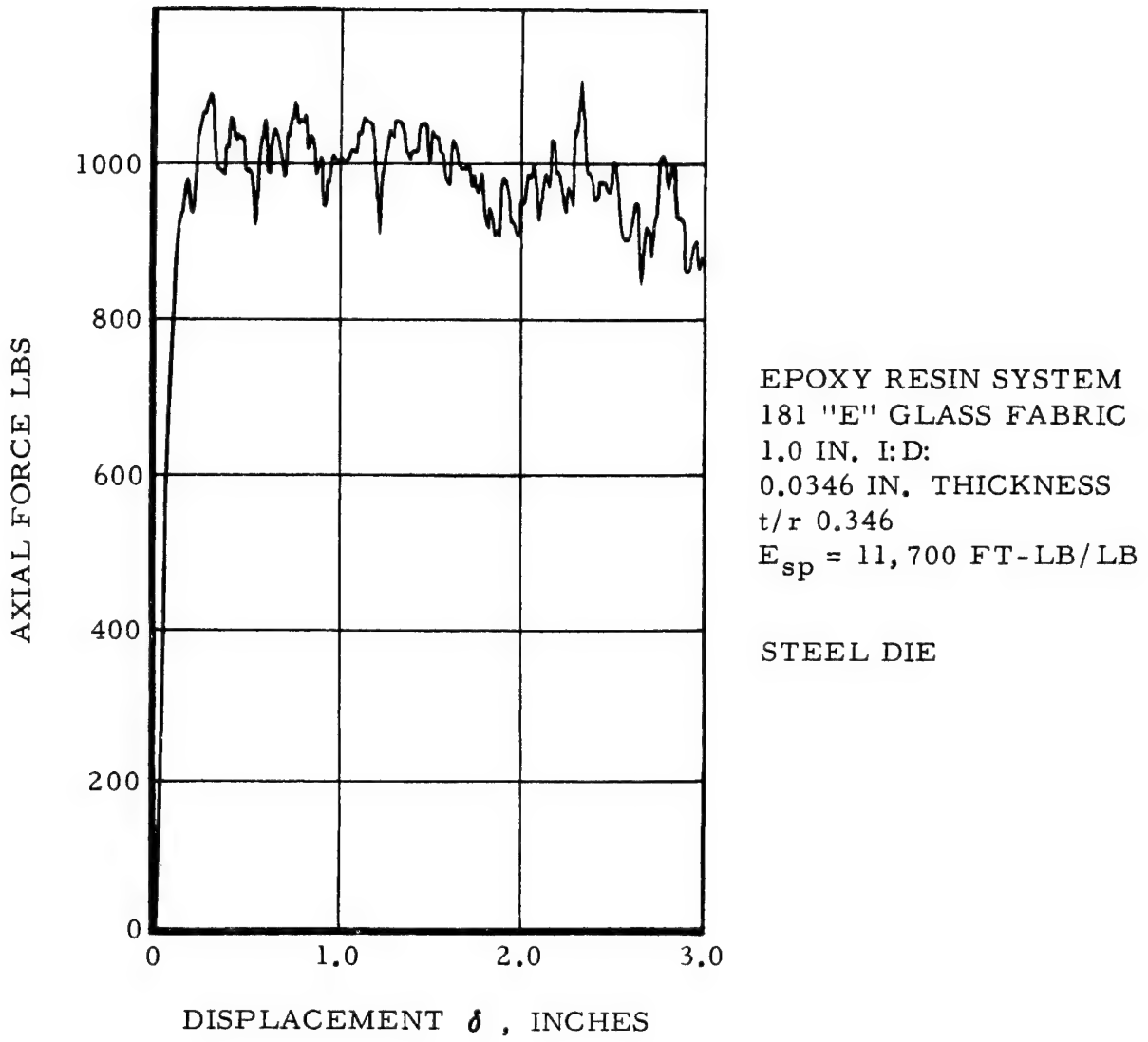

Figure 22. Typical Radio Frequency Transparent Load Displacement Graph for Epoxy Resin System Glass Fiber Reinforced Plastic Tube Fragmented over a Steel Die

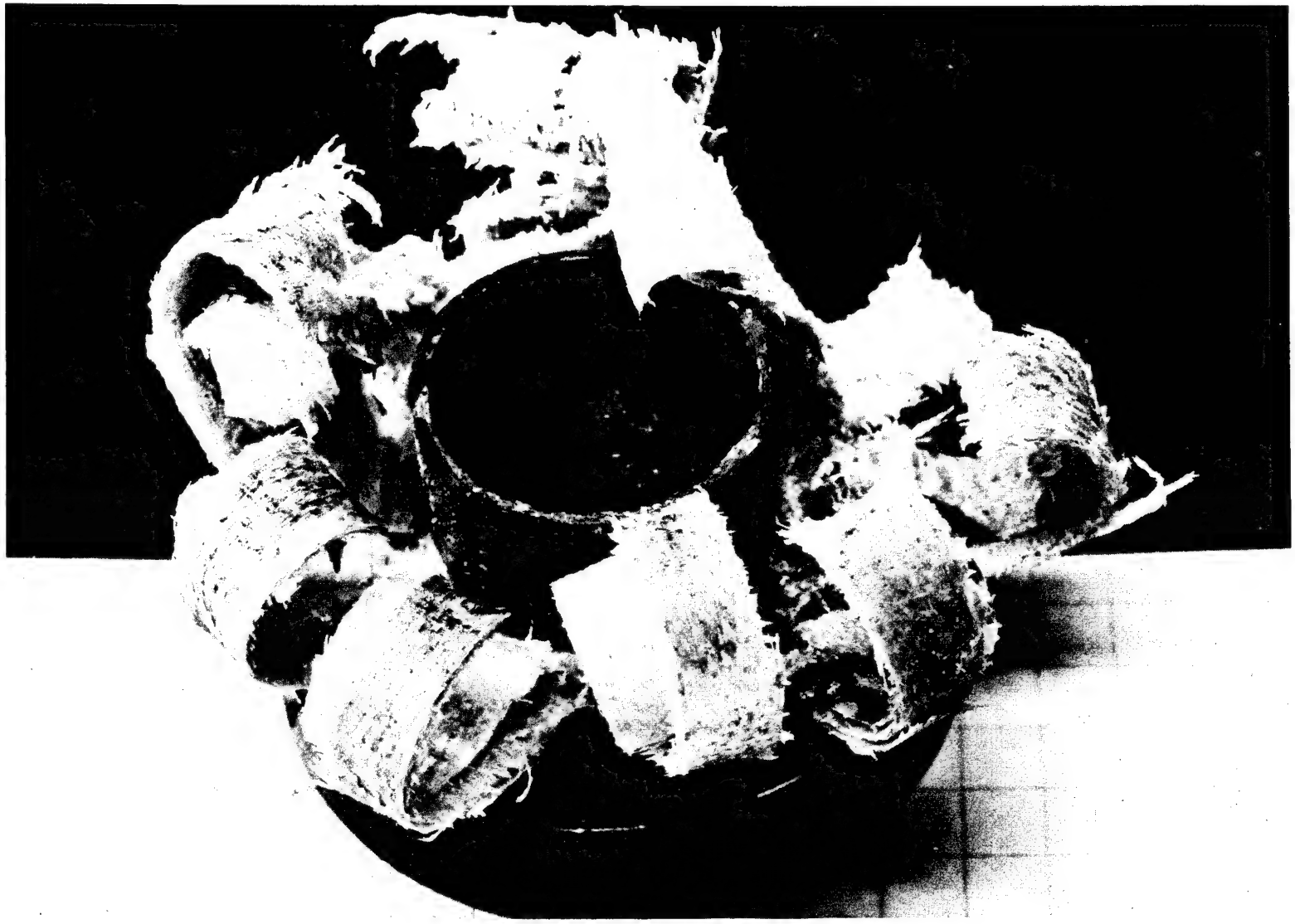

Figure 23. Specimen Constructed of 143 "E" Glass Fabric and Epoxy Resin, 3 Plies with Strength in Longitudinal Direction, 1 Ply with Strength in Hoop Direction, Loaded at 20 Inches Per Minute

RADIO FREQUENCY TRANSPARENCY TESTS

General Requirements. - The principal objective of this program is to develop an efficient energy absorption structural element which will also be radio frequency transparent within specified limits. The structural elements which were tested for radio frequency transparency were open cell elements and solid materials. The open cell types were nylon phenolic honeycomb and epoxy resin system glass-fiber-reinforced tubing. The solid materials were syntactic foam material, glass macro-balloons and epoxy resin matrix, and nylon phenolic honeycomb filled with syntactic foam. The factors which influence the radio frequency (rf) power transmission through a dielectric body include the frequency of the rf energy, the angle of incidence of the incoming wave, and the dimensions of the dielectric material. The specified rf parameters were as follows:

1. Radio frequency range: 100 to 2000 megacycles
2. Dielectric constant range: 1.0 to 10.0
3. Loss tangent range: 0.03 to 0.05.

In general, it can be stated that for maximum power transmission the energy absorption materials should have the lowest possible dielectric constant and loss tangent.

Test Set-Up and Procedure. - The test program was planned to establish the radio frequency transparency of crushed and uncrushed selected structural elements. Since the dielectric constant and loss tangent for the uncrushed materials were available from the materials producers, these known parameters were utilized in a rf attenuation equation to determine attenuation over the specified band of frequencies for the uncrushed elements. The test program was limited, therefore, to the determination of the attenuation over the specified band of frequencies for the crushed materials.

The material's coaxial test fixture which was used for testing the four material types is shown in Figure 24. This fixture,

which is a 50-ohm, solid-air coaxial transmission line, is one meter is length, and has GR fittings at each end. When testing a given sample, the crushed material was inserted as uniformly as possible between two plexiglass discs as shown. The actual length of the material sample can be accounted for in the rf insertion loss equation; however, one meter length makes the calculation more expeditious. In addition, for low loss materials, too short a length yields absolute loss values less than the accuracy of the equipment setup.

The relationship of the coaxial fixture with the rest of the test set-up is shown schematically in Figure 25. The rf insertion loss of one meter length for the test sample can be determined from the following relation:

$$L_s = P_i - (P_o + P_r)$$

where

L_s = sample rf insertion loss in db

P_i = input power level in dbm

P_o = output power level in dbm

P_r = reflected power level in dbm

The schematic test setup in Figure 25 indicates the three positions of the power meter so that P_i , P_o , and P_r can be obtained for computation of the test sample rf loss L_s in the above equation. The actual laboratory test setup for this schematic system is shown in Figure 26. The power meter is shown centered behind the 1-meter, 5/8-inch coaxial line. The input and output couplers are shown at the edge of the bench at each end of the coaxial test fixture. The signal generator is located behind and slightly to the right of the power meter on the shelf above the test bench.

Discussion of Results. - Prior to the rf testing of the four crushed specimens, an rf attenuation measurement was conducted on a nylon rod. This test was conducted to establish the degree

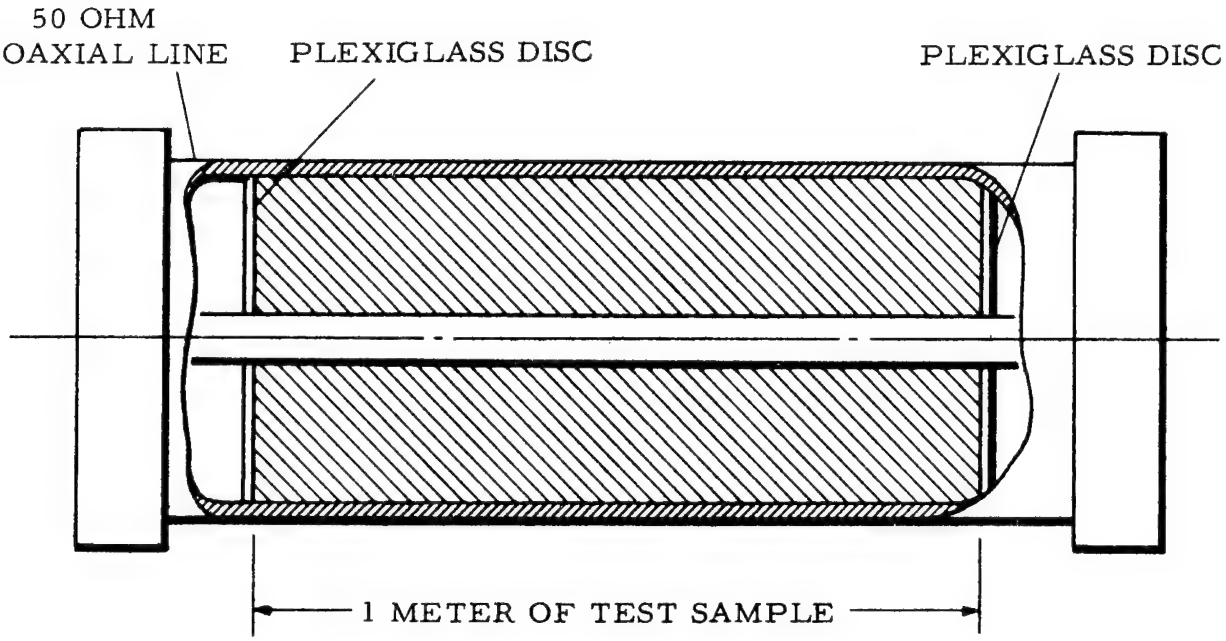

Figure 24. Coaxial Line Test Fixture with Inserted Test Sample

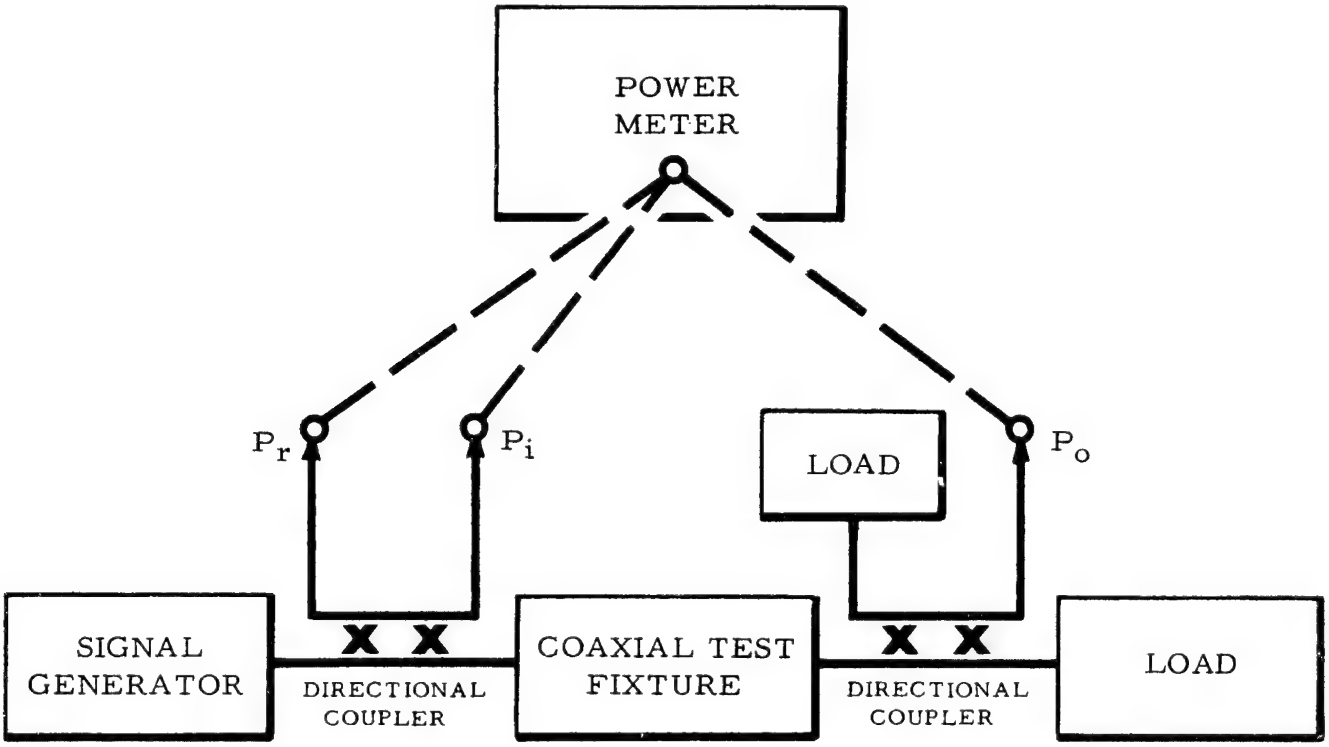

Figure 25. Schematic of the Electrical Test Setup

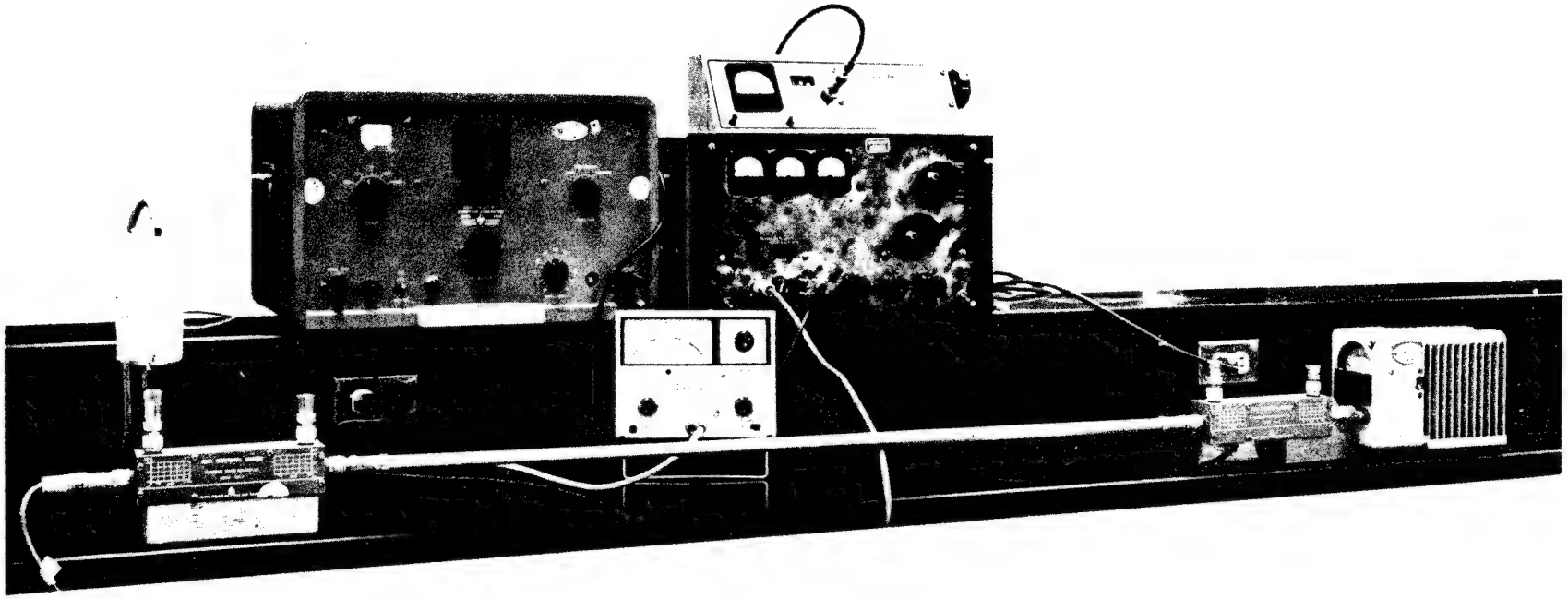

Figure 26. Electrical Test Set Up

of correlation between experimental and predicted attenuation characteristics of a known solid material. The results are presented with attenuation as a function of frequency over most of the 100 to 2000 megacycle spectrum (Figure 27). The results indicated agreement to within less than 1 db about the predicted amount of insertion attenuation which is within the accuracy of the test setup measurements.

The attenuation as a function of frequency over most of the 100 to 2000 frequency range is presented in Figure 27 for two open cell type materials, crushed 3/16-in cell size nylon phenolic honeycomb, and fragmented 1.0-inch-diameter epoxy resin system glass-fiber-reinforced tubing. A similar attenuation variation with frequency is shown for two closed cell or solid materials in Figure 28. This latter presentation shows both crushed syntactic foam and crushed nylon phenolic honeycomb filled with syntactic foam. The test results are shown with connected test points, the other plot is a predicted attenuation with a $\pm$ 1 db upper and lower limit of measurement accuracy also plotted about this calculated line. If it is assumed that the power meter exhibits an accuracy of $\pm$ 0.5 db and that any power drift of the signal generator remains within 0.5 db of its original setting while the power measurements are made as previously described, then a measurement accuracy of $\pm$ 1 db is reasonable. The predicted curves in each of these graphs were determined by calculating the dielectric constant and loss tangent values from Appendix B equations (7) and (11), respectively, of open cell crushed material, honeycomb and tubing, and using these parameters in equation (4) or nomograph Figure B-1 of Appendix B to calculate attenuation for a range of frequencies. Similarly, for the closed cell or solid materials (syntactic foam and honeycomb filled with syntactic foam), Appendix B equations (5) and (10) are used for dielectric constant and loss tangent, respectively, in equation (4) or Figure B-1 nomograph. The materials producers' dielectric constants and loss tangents for

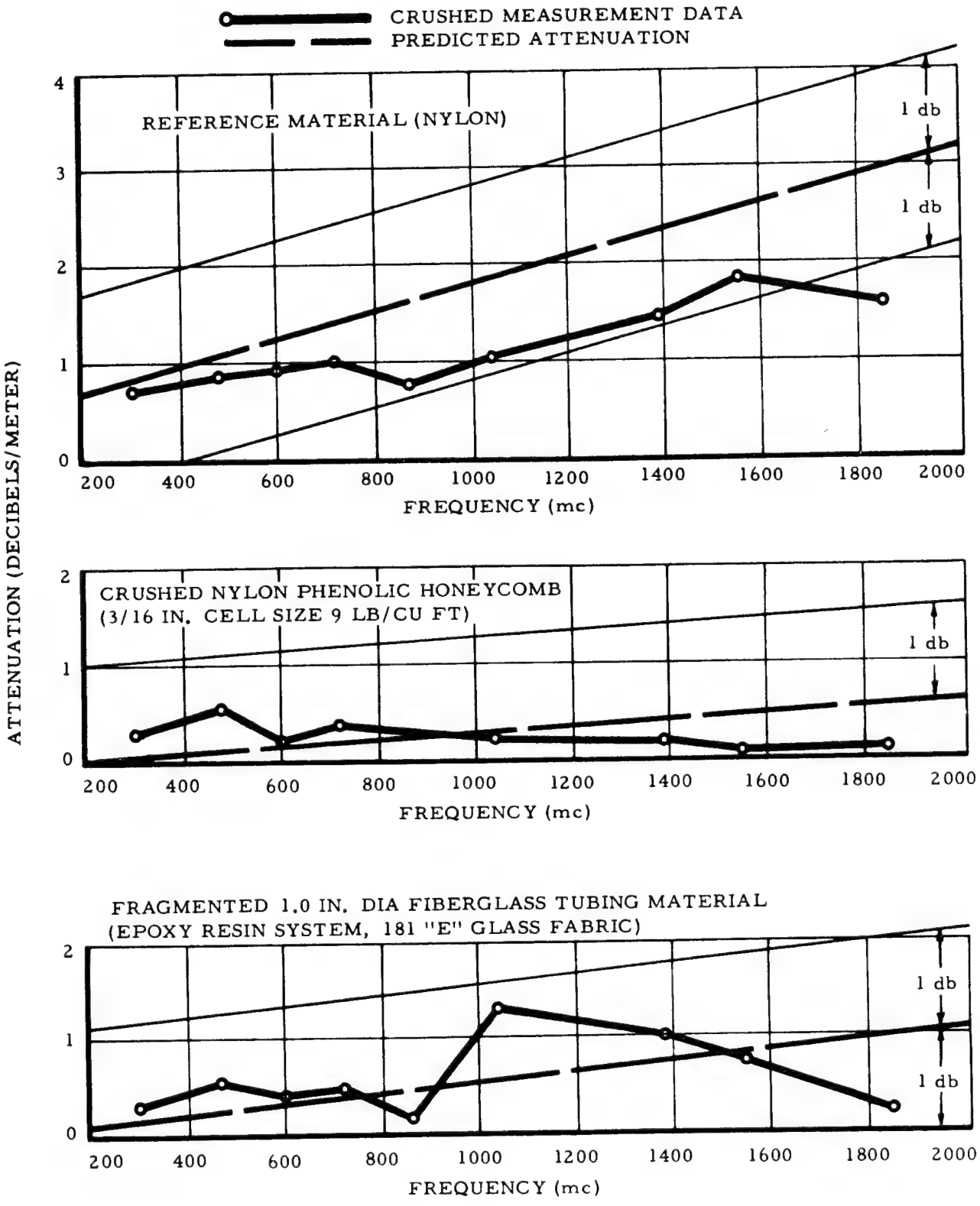

Figure 27. Material Attenuation Characteristics

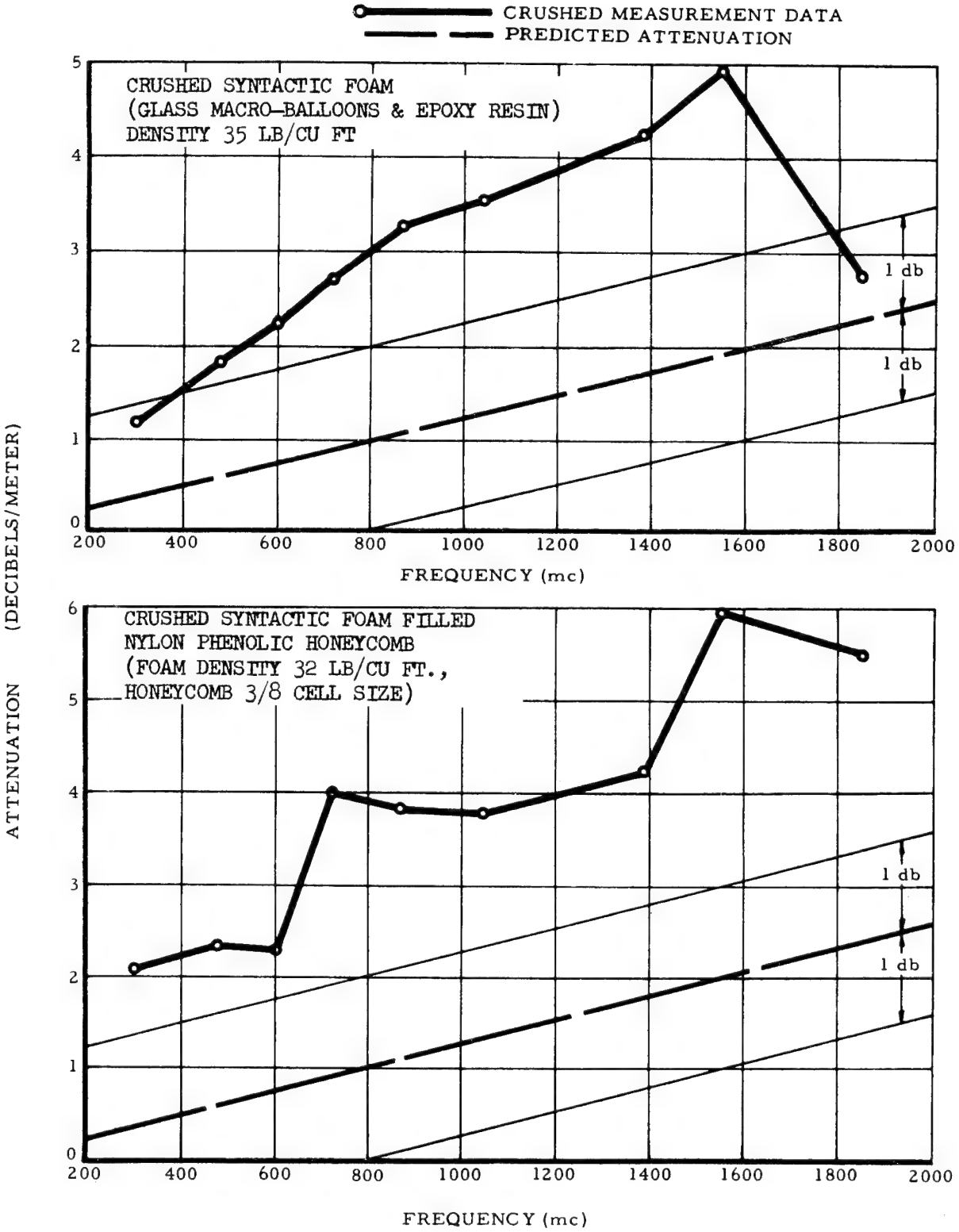

Figure 28. Material Attenuation Characteristics

the materials and the calculated crushed element values are tabulated in Table VII.

TABLE VII

MATERIAL CHARACTERISTICS FOR ATTENUATION PREDICTION

Element	Dielectric Constant		Loss Tangent	
	Element Material	Crushed Element	Element Material	Crushed Element
Nylon Phenolic Honeycomb	1.07*	1.21	.0010*	.0028
181 Fabric Epoxy Resin Laminate Tube	4.15*	1.33	.0240*	.0048
Syntactic Foam	1.62	1.51	.0123	.0105
Epoxy resin	1.80*		.0150*	
Glass macro-balloons	1.25*		.0100*	
Nylon Phenolic Honeycomb & Foam	1.58	1.54	.0119	.0113

*Materials producer data: All other values tabulated are calculated.

Agreement between measured and predicted values as presented on the graphs for open cell materials such as the nylon phenolic honeycomb and the fiberglass tubes is close. These materials and elements were also the most mechanically efficient as energy absorbers. The comparisons between calculated and measured values for the solid materials such as the syntactic foam and the foam-filled honeycomb showed that the measured level of rf insertion loss was approximately 3/4 to 1 db above the measurement error tolerance limit level over most of the frequency range. This difference may be due to the fact that the materials producers quoted constant values for ϵ' and tan δ for syntactic foam listed in Table VII for the entire range of frequencies when it has been observed that these properties may vary with frequency.

CONCLUSIONS

The results of all the tube fragmenting tests for both the hand- and tape-wrapped tubes are presented with the parameter t/r as a variable in Figure 29. The epoxy resin systems are distinguished by the solid dots in the graphs. It was determined that even when the parameter t/r was plotted cubed as was done in the previous investigations for aluminum tubing there was considerable scatter in the results and the variation with $(t/r)^3$ of the fragmenting stress could not be determined from these results. When the test results were replotted using the ply thickness as a parameter (Figure 30), the results were shown to be separated into two distinct groups, a scatter band for hand-wrapped specimens and a narrow band which increased in stress level with number of plies for tape-wrapped specimens. The tests of hand-wrapped specimens were for various t/r; therefore, more scatter could be expected from these differences while the tape-wrapped tubes were tested on dies which were considered to give the near optimum ratio t/r range of approximately 0.350 to 0.400. The strength of glass-fiber-reinforced laminates has been definitely established to vary in the manner shown for the tape-wrapped tubes in Figure 30 for thicknesses of 1/4 inch (25 plies) and less, and equations are provided in MIL-HDBK-17 for expressing this variation in material strength and stiffness. It can be suggested that larger tubing with wall thicknesses which are not sensitive to this strength variation may prove to be even more efficient than the best tubes tested in this program.

A parametric design graph is presented in Figure 31 for use in determining the usable stroke of an energy absorption system when the limiting impact load factor and impact velocity is specified. This graph shows that for the specified range of 10 to 1000 g's for this program, a 12-inch usable stroke satisfies an impact velocity range of 25 to 300 feet per second. These long strokes, and longer, can be

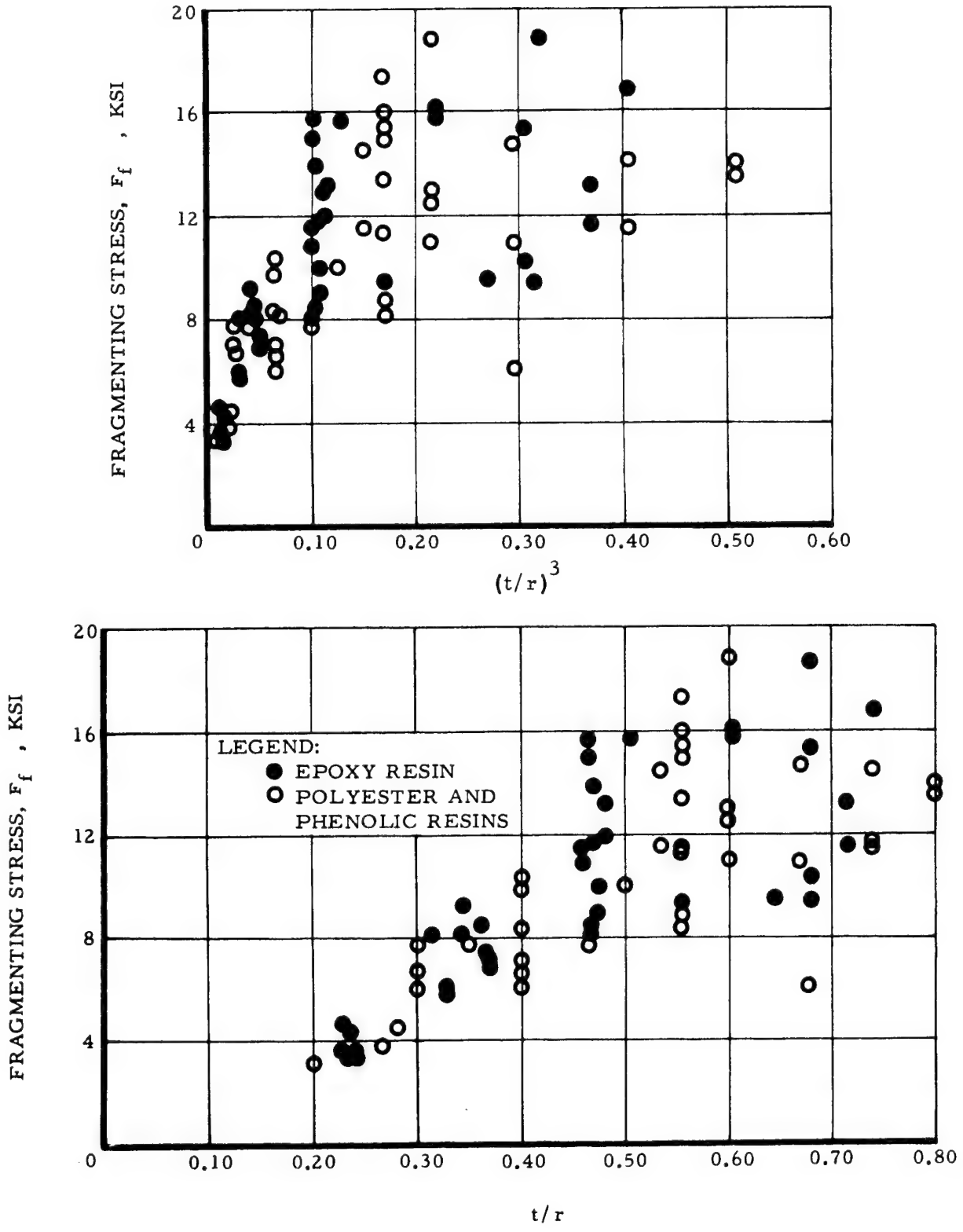

Figure 29. Variation of Fragmenting Stress for 181 "E" Glass Fabric with (t/r) Parameter

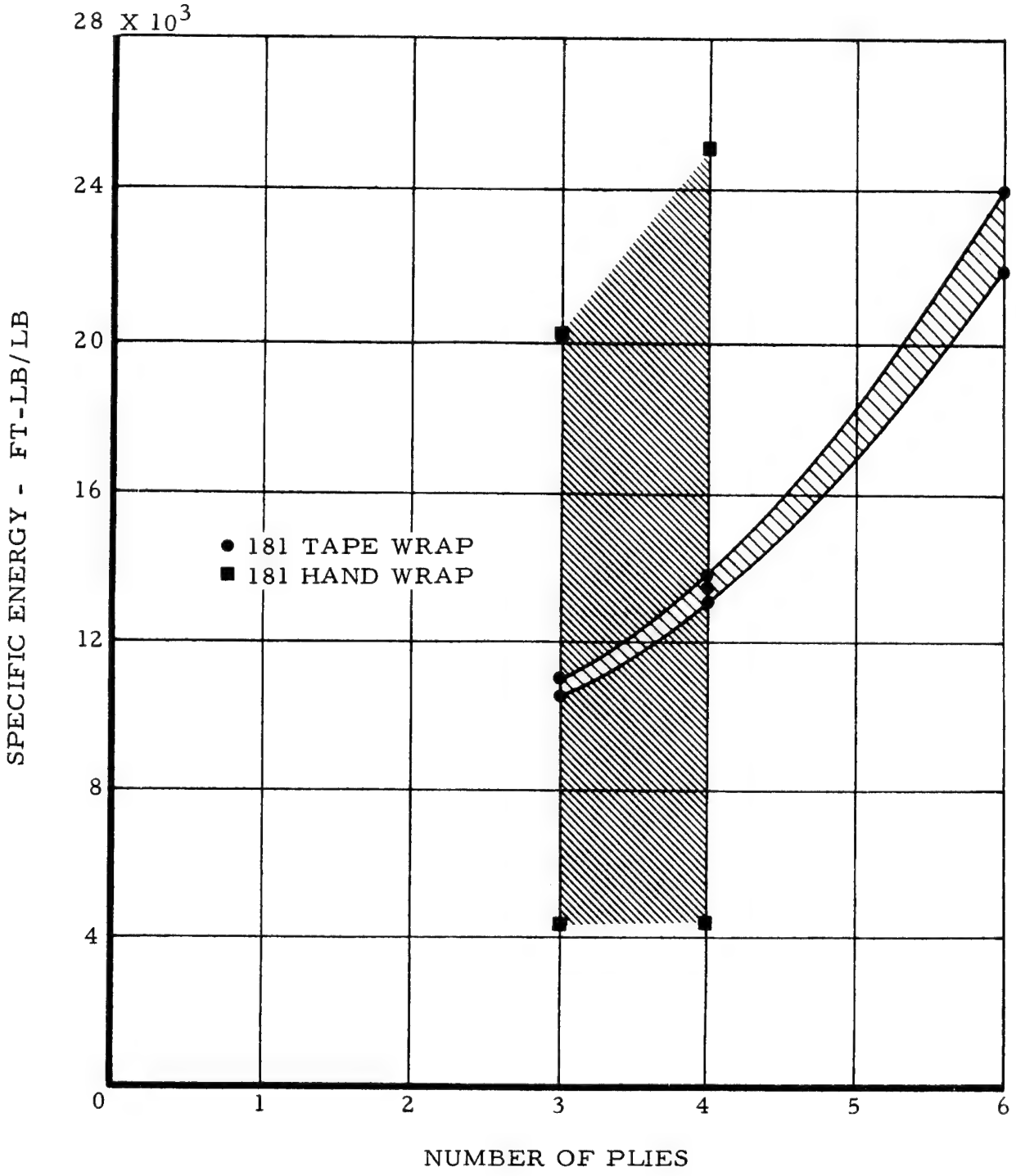

Figure 30. Variation of Fragmenting Specific Energy for 181 "E" Glass Fabric with Epoxy Resin System, as a Function of Tube Wall Thickness

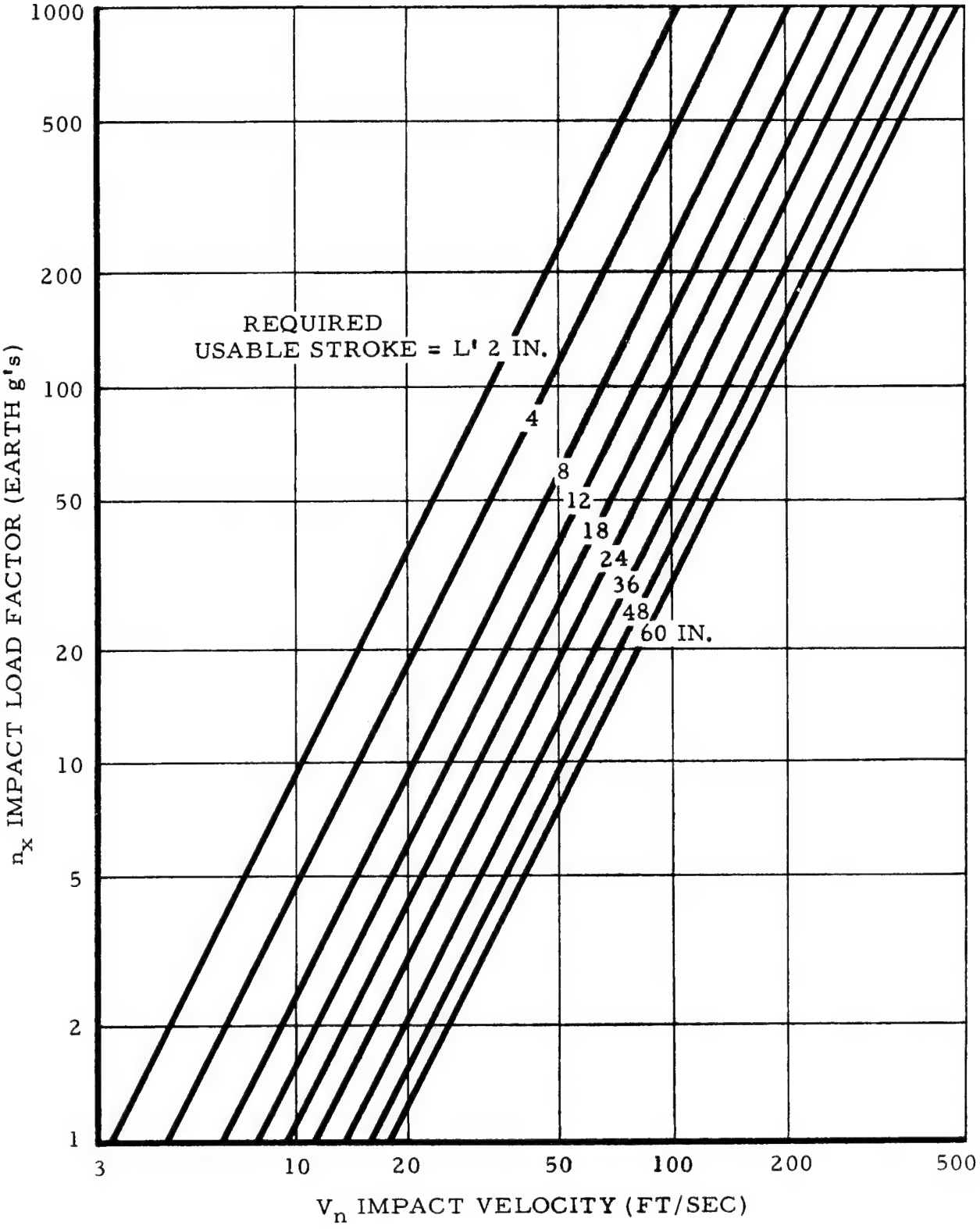

Figure 31. Determination of Required Usable Stroke for Energy Absorption Systems

more easily handled by fragmenting tubes than in crushing honeycomb, but this program has demonstrated that both structural elements are efficient radio-frequency-transparent, energy-absorption systems.

The results of the honeycomb crushing tests and the tube fragmenting tests are presented as design type graphs in Figures 32 and 33, respectively. The procedure for using the honeycomb material in design would be to first use Figure 31 to establish usable stroke length. From Figure 32, after the payload weight (W) has been multiplied by the limiting impact load factor (n_x) and divided by the cross sectional area to be covered by the honeycomb (A), the crushing strength (F_{cc}) determined from these parameters is used to enter the graph and read the required density from the curve for nylon phenolic honeycomb. Adjustments can be made on the honeycomb area (A) and density until the point on the curve coincides with available cell size material. A similar design procedure can be used with the tube fragmenting bar chart shown in Figure 33. The payload weight is multiplied by the impact load factor and then in this case is divided by an estimated number of tubes to be used for the fragmenting process. When the chart is entered with this parameter, the number of plies for 181 fabric epoxy resin system tubing of 1.0-inch inside diameter are determined as is also the weight per inch of tube length. If additional tube sizes are tested these can be added to this chart to make it more complete. A rapid calculation of energy absorption system weight can be made for these two energy absorption structural element types by the use of Figures 32 and 33.

The results of this experimental investigation have established that both the tape-wrapped glass-fiber-reinforced plastic tubing when fragmented over a die and the nylon phenolic honeycomb when crushed represent efficient methods of energy absorption for structural elements which are also radio frequency transparent.

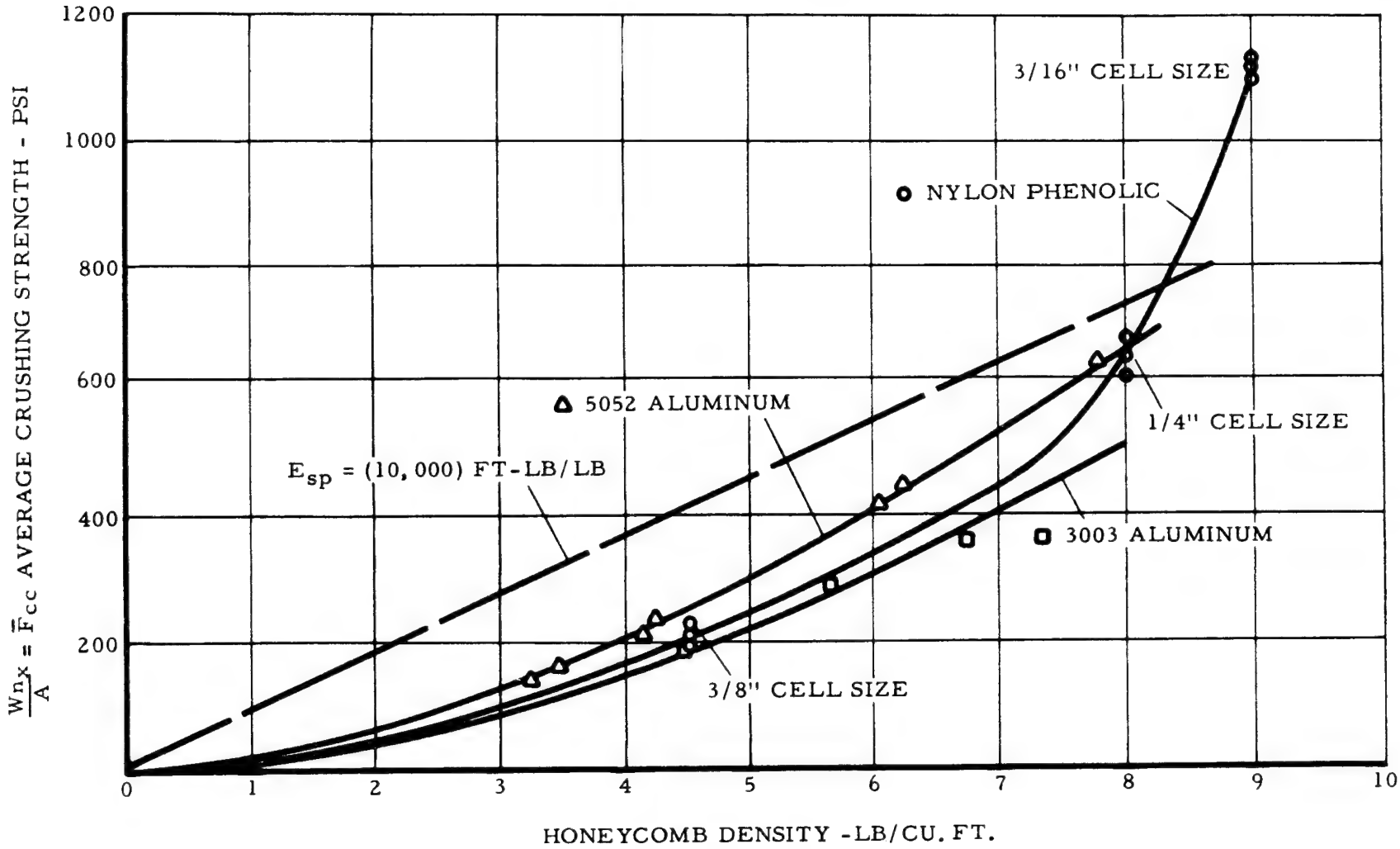

Figure 32. Design Chart to Determine Single Lap Honeycomb Density and and Geometry Required for a Specified Average Crushing Strength

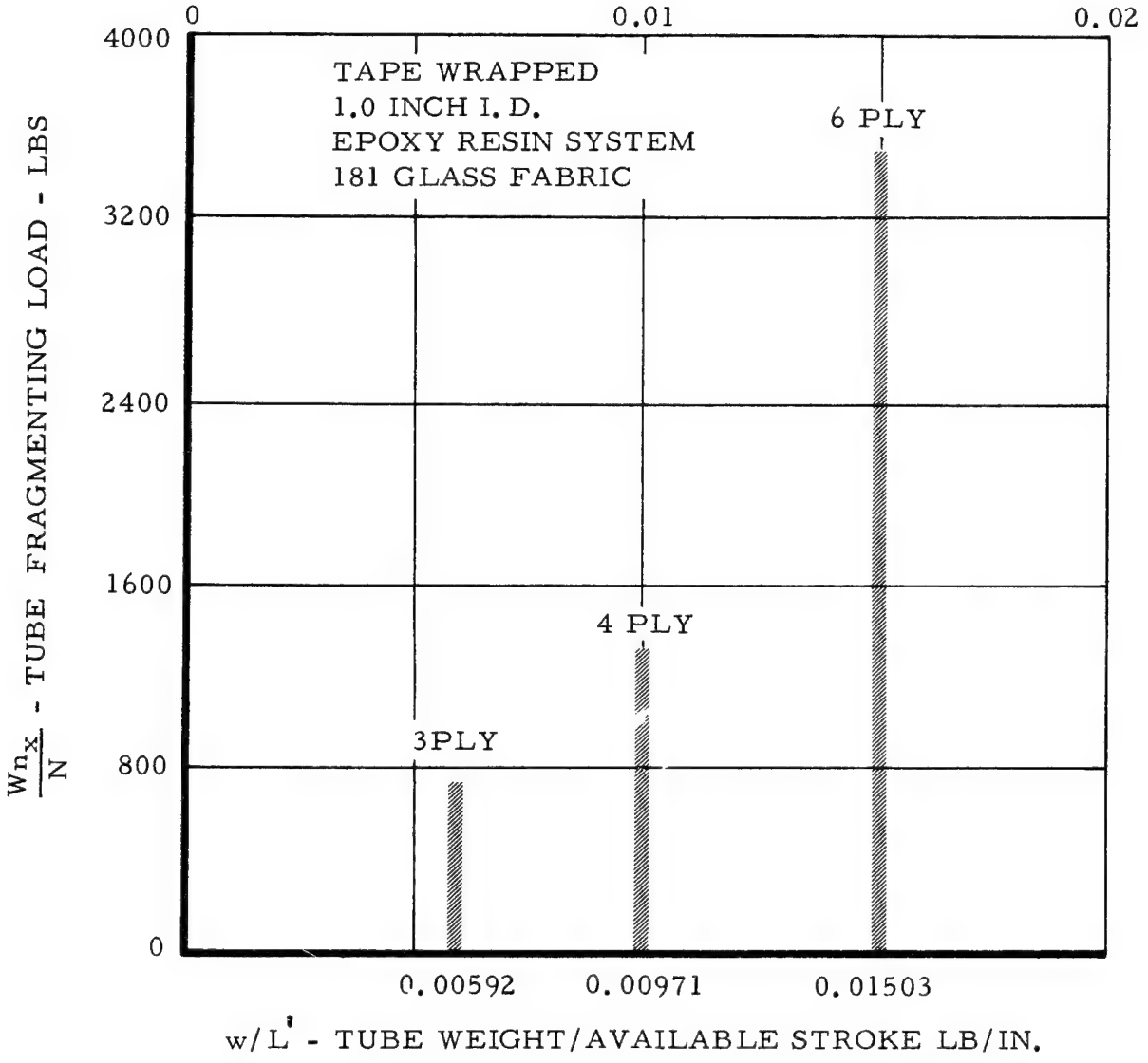

Figure 33. Design Chart to Determine Fragmenting Tube Required Properties and Geometry for Specified Average Fragmenting Load Per Tube

The results of this program have established that the tape-wrapped glass-fiber-reinforced plastic tube when fragmented over a die is competitive with the most efficient aluminum tube energy absorption process. It was also established that both the GRP tube process and the crushing of nylon phenolic honeycomb represent efficient methods of energy absorption at rates of 1.0 inch per minute, and that these structural elements are radio-frequency transparent before and after energy absorption.

The application of new mechanical deformation types of energy absorption processes requires consideration of the actual mission environment of spacecraft landing systems, such as actual landing impact velocities, impacting with horizontal components of velocity, and exposure of landing systems to temperature before landing. In addition, there are newer plastic materials, new glass reinforcements, and other structural geometries to consider before efficient radio-frequency-transparent energy systems can be developed for a vehicle system. In order to realize the potential of these new processes, a supplementary research program is recommended which embodies the following tasks:

1. Additional element tests of newly developed high-temperature resin systems and of new non-woven and woven glass fabrics as tubing of varying diameters and as honeycomb elements. These additional element tests would include impact loading rates corresponding to the actual landing system environment. High temperatures would also be simulated corresponding to eventual systems applications.

2. Using the developments from the program reported herein and the one stated in Item 1, application of the tube fragmenting and honeycomb crushing processes to actual landing system design for representative spacecraft.

The systems would be designed to use the elements most effectively for oblique angle of impact and tests would be conducted so as to demonstrate the adequacy of the system concept using these elements.

APPENDIX A

Material Range of Application. - The range of application of any impact absorber is a function of certain measurable parameters associated with the impact absorption material and the impact absorption process. Figure A-1 shows typical load-deformation curves for various energy absorbers. For an ideal energy absorber the energy normal to the surface $\left(\frac{1}{2} m \ V_n^2\right)$ is assumed to be absorbed, so that

$$\frac{1}{2} m V_n^2 = \int_o^L P dx = \bar{P} L, \tag{1}$$

and

$$\bar{P} = \frac{\frac{1}{2} m V_n^2}{L} \tag{2}$$

Since the force $\bar{P}$ is constant for an ideal energy absorber, and the velocity V_n is assumed to be reduced to zero in stroke L,

$$V_n^2 = 2aL \tag{3}$$

or

$$a = \frac{V_n^2}{2L} \tag{4}$$

If we assume that the energy absorber is one in which the material is crushed (such as plastic foam or honeycomb material), then

$$\bar{P} = \bar{F}_{cc} A; \tag{5}$$

or

$$A = \bar{P}/\bar{F}_{cc}, \tag{6}$$

where $\bar{F}_{cc}$ is the crushing stress and A is the contact area.

For real impact absorption materials, the actual load-deformation curve may be approximated as shown below.

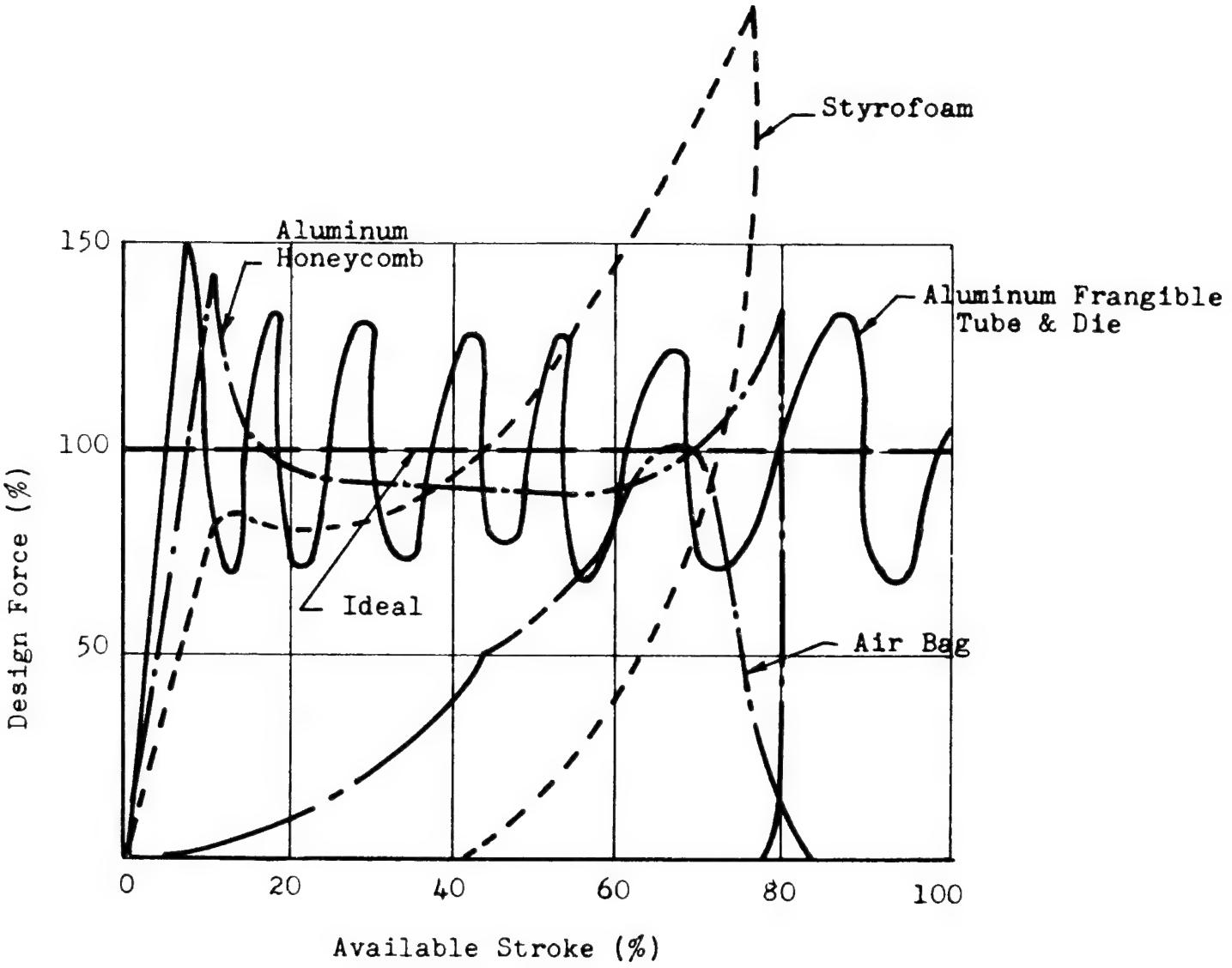

Figure A-1. Typical Load-Deformation Curves for Various Energy Absorbers

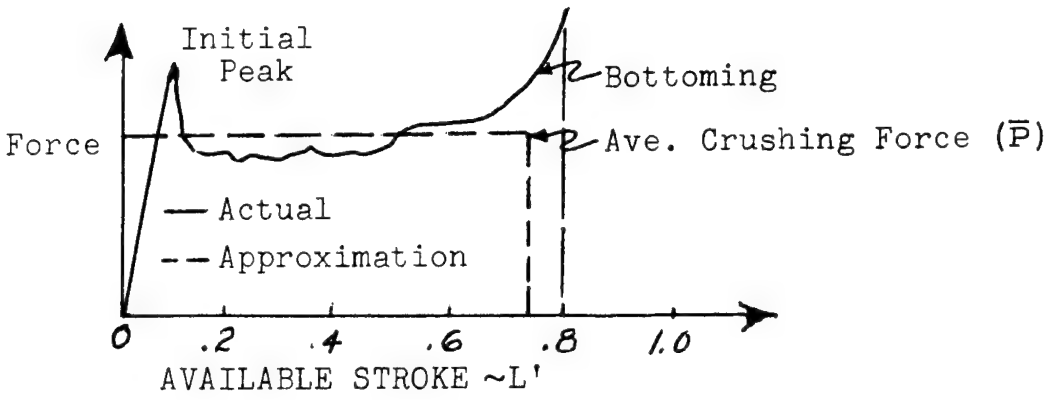

Since for many crushable impact absorption materials the usable stroke L is approximately 75 percent of the available stroke L', the available stroke is set at 4/3 L. Then the volume V of the impact absorption material is

$$V = A\,(4/3L) \tag{7}$$

If ρ is the density of the impact absorption material, then the earth weight of this material, w, is

$$w = V\rho = \left[A(4/3L)\right]\rho . \tag{8}$$

Combining Egs 2, 6 and 8,

$$w = (\bar{P}/\bar{F}_{cc})\,(4/3L)\rho = \frac{\frac{1}{2} m V_n^2}{L\,\bar{F}_{cc}}(4/3L)\rho ,$$

or

$$w = \frac{2}{3}\,\frac{W}{32.2}\,V_n^2 \Big/ \bar{F}_{cc}/\rho , \tag{9}$$

where W = total earth weight of impacting vehicle, lbs.

The quantity $(\bar{F}_{cc}/\rho)$ is the ideal specific energy absorption capacity E_{sp} of the material, measured in ft-lb/lb, so that

$$E_{sp} = \frac{\bar{P}L}{\rho AL} = \frac{\bar{P}/A}{\rho} = \frac{\bar{F}_{cc}}{\rho} \tag{10}$$

Equation 9 may be written as a weight fraction w/W, which represents the fraction of the total weight of the impacting vehicle required for impact absorption material, so that

$$\frac{w}{W} = \frac{2}{3}\,\frac{1}{(32.2)}\,\frac{V_n^2}{E_{sp}} = 0.0207\,\frac{V_n^2}{E_{sp}} \tag{11}$$

Equation 11 is shown plotted versus impact velocity V_n for several different honeycomb and plastic foam materials in Figure A-2. Also plotted are the weight fractions for aluminum frangible tube and nylon air bags. Since the frangible tube process can utilize 100 percent of the available stroke, the weight fraction relation for this material is given by

$$\frac{w}{W} = \Big/_{\text{frangible tube}} \frac{1}{2(32.2)} \frac{V_n^2}{E_{sp}} = 0.0155 \frac{V_n^2}{E_{sp}} \qquad (12)$$

The curves presented in Figure A-2 are idealized, in that the weight fractions include only the impact absorption material and do not include the weight fraction of additional components* that may be required for proper operation of a real impact absorption system.

It is important to note that Figure A-2 presents a weight fraction, based on unidirectional impact of the lander vehicle. Furthermore, it is assumed that all the impact absorption material carried by the lander vehicle is fully utilized in the landing impact. For the case of a lander vehicle capable of landing in any attitude, it is obvious that redundancy of impact absorption material is necessary. If it is assumed that the lander vehicle is spherical, with the impact-absorption system completely surrounding the vehicle (as shown in Figure A-3), the impact absorption redundancy factor is calculated to be

$$\text{Redundancy Factor} = \frac{w}{w'} = \frac{2}{1 - \cos \frac{\phi}{2}} \qquad (13)$$

where: w = total weight of impact-absorption material, lbs

w' = weight of effective impact-absorption material, lbs

ϕ = spherical angle of impact absorption material effectiveness, degrees

* By "additional components" is meant the dies for operation of frangible tube devices, load distribution plates for honeycomb or foamed plastic material, air blowers or compressed air bottles for air bags, etc.

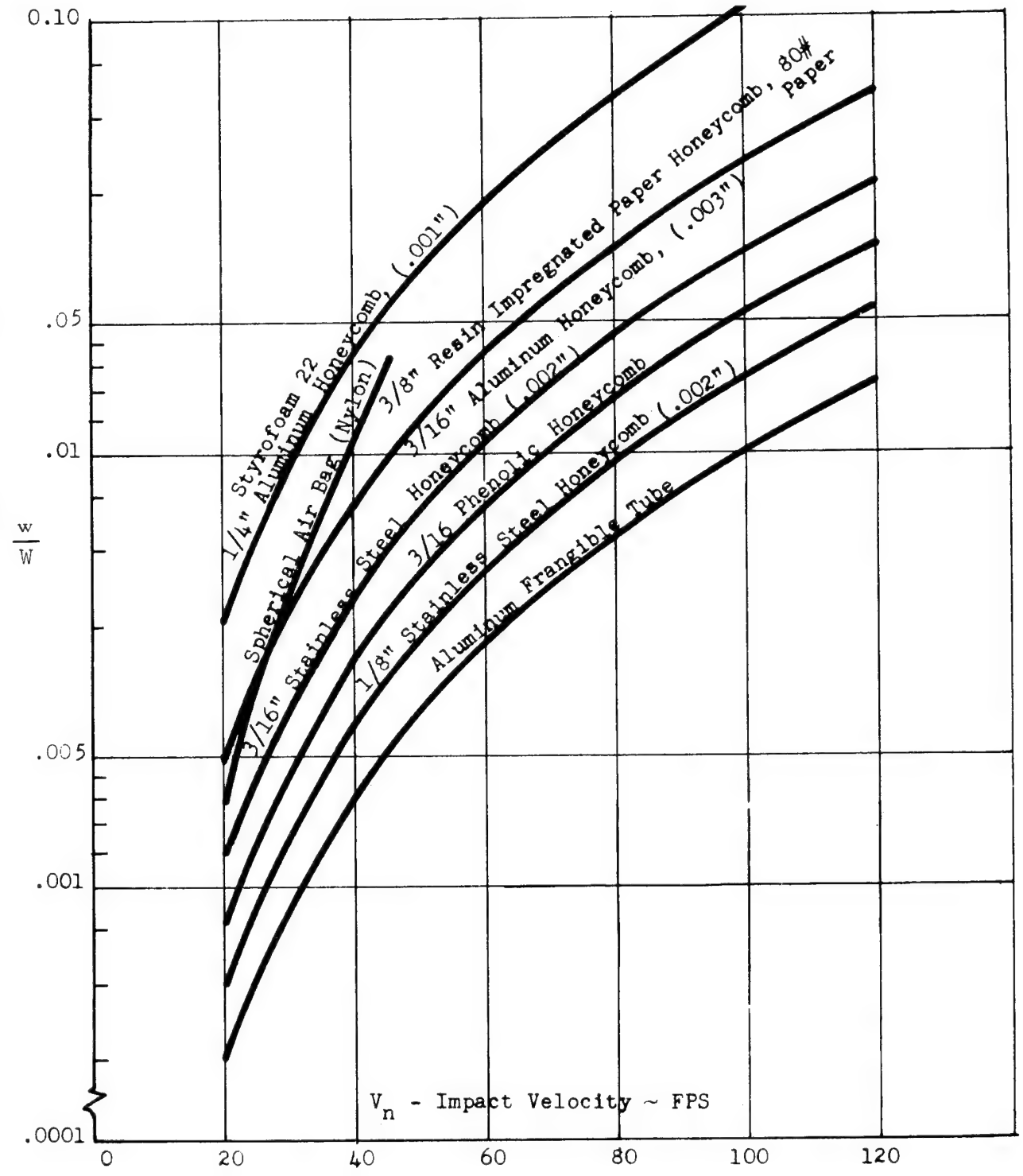

Figure A-2. Idealized Weight Fraction Versus Impact Velocity for Various Impact Absorption Materials and Devices - Unidirectional Impact

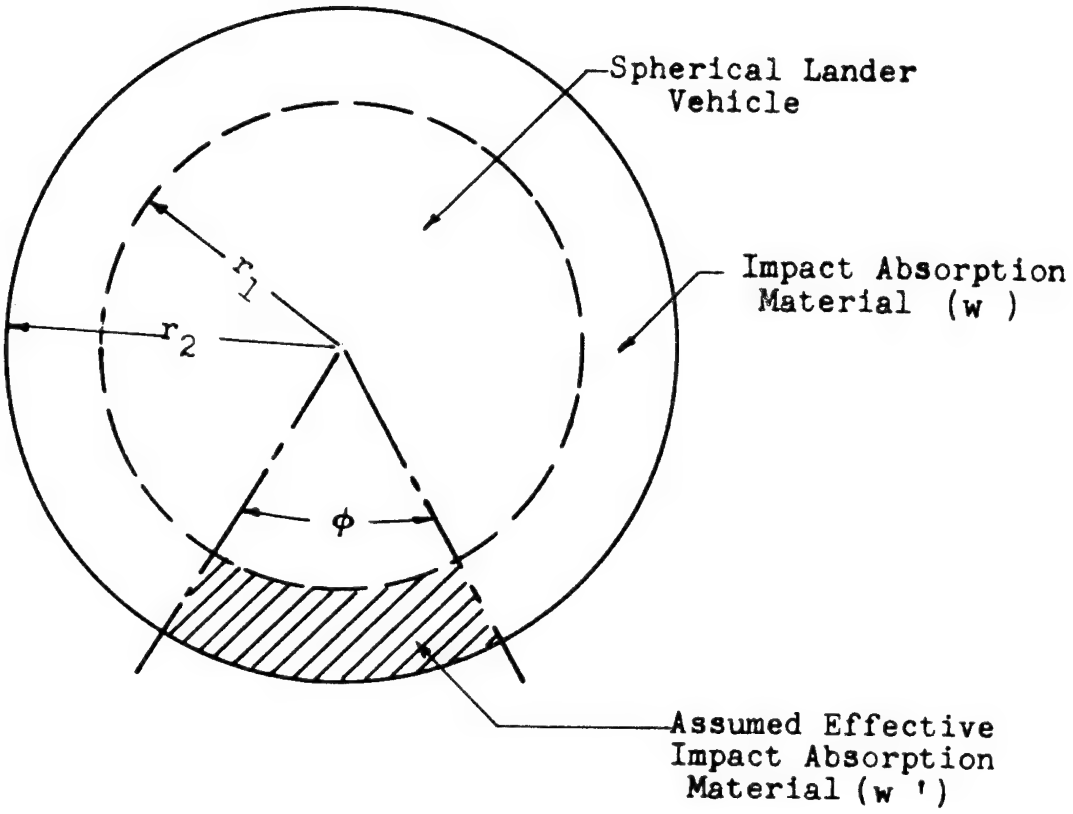

$$w = \frac{4}{3}\pi\rho(r_2^3 - r_1^3)$$

$$w' = \frac{2}{3}\pi\rho\left[\left(1 - \cos\frac{\phi}{2}\right)\left(r_2^3 - r_1^3\right)\right]$$

$$\frac{w}{w'} = \text{Redundancy Factor} = \frac{4/3\pi\rho\ (r_2^3 - r_1^3)}{2/3\pi\rho\left[\left(1 - \cos\frac{\phi}{2}\right)\left(r_2^3 - r_1^3\right)\right]}$$

$$\text{Redundancy Factor} = \frac{2}{1 - \cos\frac{\phi}{2}}$$

Figure A-3. Required Redundancy of Impact Absorption Material for a Spherical, Omnidirectional Lander Vehicle

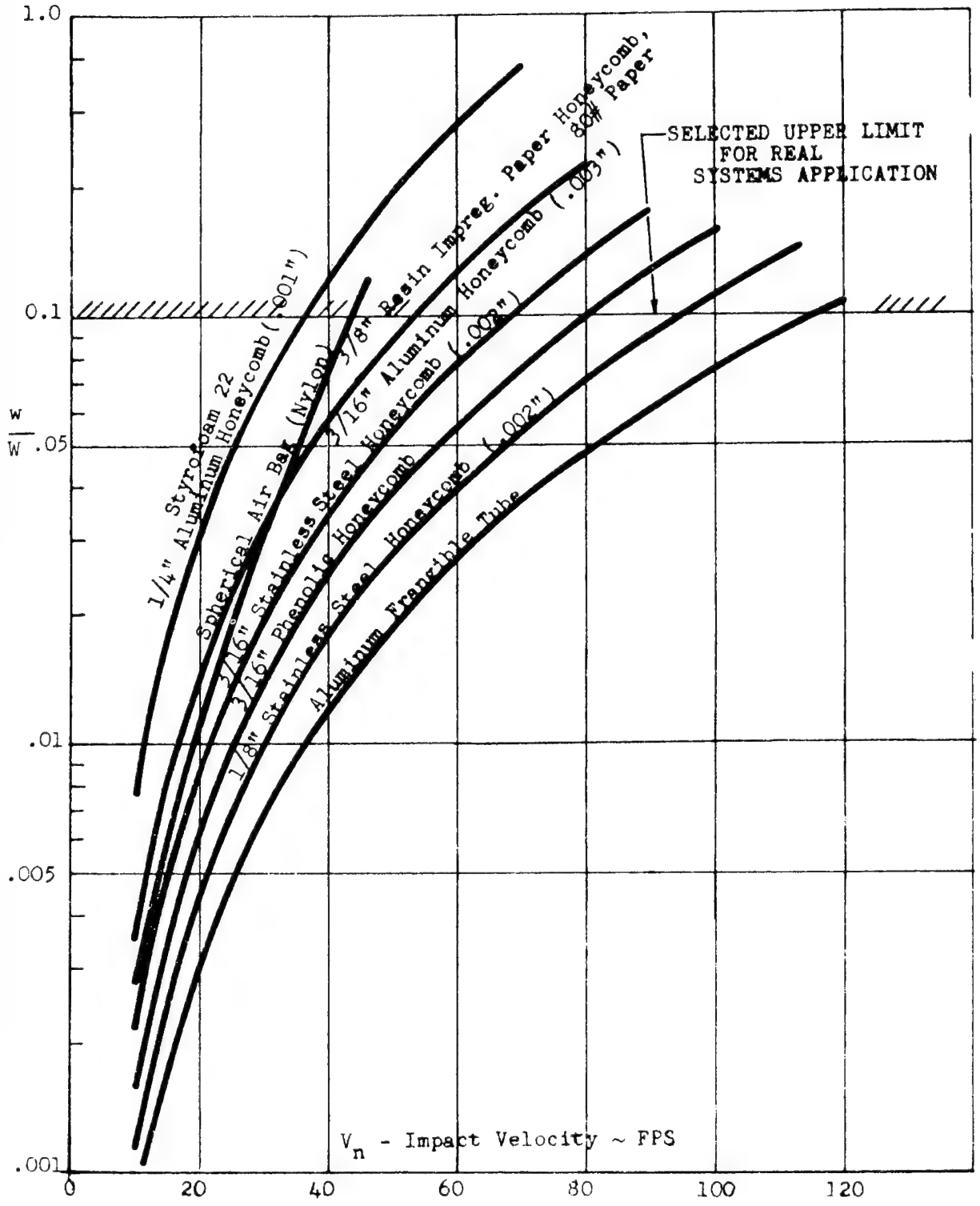

Figure A-4. Idealized Weight Fraction Versus Impact Velocity for Various Impact Absorption Materials and Devices - Omnidirectional Impact for a Spherical Lander Vehicle -- Redundancy Factor = 15

If ϕ is set equal to 60 degrees, a value felt to be compatible with honeycomb and frangible-tube type impact absorbers, the redundancy factor is

$$RF = \frac{2}{1 - \cos 30°} = 15$$

Figure 4 presents the weight fractions of impact-absorption material for a spherical, omnidirectional lander vehicle. The various curves are those presented in Figure A-2, increased by the stated redundancy factor. In Figure A-4 a value of 0.10 (10%) was selected as an upper limit for any real system application. With such a limit, it is possible to establish a practical upper limit for the impact velocity for each type of impact absorber.

APPENDIX B

Rf Loss Determination of Dielectric Materials. - There are two primary electrical parameters which define the absolute dielectric constant of a non-magnetic isotropic material. These are the real relative dielectric constant, ϵ', and the relative loss factor, ϵ'', which are related to the relative absolute complex dielectric constant, ϵ^*, as follows:

$$\epsilon^* = \epsilon' - j\,\epsilon'' \tag{1}$$

The term ϵ' is associated with the ability of the dielectric material to store energy and ϵ'' is associated with the dissipation which occurs in the material. From knowledge of these two parameters, another useful parameter, the loss tangent ($\tan \delta$), is utilized to define the quality factor, Q, of the material where

$$Q = \frac{1}{\tan \delta} \tag{2}$$

and

$$\tan \delta = \frac{\epsilon''}{\epsilon'} \tag{3}$$

The techniques and methods to be employed for determining these primary electrical parameters of crushable rf materials for the development of a radio frequency transparent, energy absorbing, structural element involves a standard test method which employs the use of a nomogram.

A. Von Hipple has derived a universal normalized equation which relates the dielectric constant and loss tangent of a material at any given operating wavelength, λ_o, in meters as follows:

$$\begin{aligned} \text{rf insertion loss} &= 8.686 \left(\frac{2\pi}{\lambda_o}\right) \left[\frac{\epsilon'}{2}\left(\sqrt{1+\tan^2\delta}-1\right)\right]^{1/2} \frac{\text{db}}{\text{meter}} \\ &\cong \frac{8.686\,\pi \tan\delta \sqrt{\epsilon'}}{\lambda_o} \end{aligned} \tag{4}$$

This equation has been nomographed and is reproduced as shown in Figure B-1 for low-loss dielectrics. It should be noted in this nomogram that ϵ'/ϵ_o is defined as the relative dielectric constant and μ/μ_o is the relative permeability (one for nonmagnetic materials).

However, in order to expedite measurements on crushable rf-transparent materials most economically, it was decided that the rf insertion loss measurements be made only on crushed samples. Since the relative dielectric constant and loss tangent of the standard materials utilized are known parameters, the rf insertion loss over a band of frequencies can be computed or predicted from the nomograph in Figure B-1. Consequently, if the insertion loss characteristic of each material in a crushed state is determined by measurement, a comparison analysis can then be made of the effects on a particular material in its crushed state with its static or uncrushed state.

The predicted loss of any given material is readily determined from the nomogram as follows. The choice of dielectric material specifies the value of the dielectric constant and the loss tangent (two points on the right hand vertical line). At some particular operating frequency or wavelength, the rf insertion loss through 1-meter thickness of the material can then be determined by noting the proper intersecting points on each of the three vertical lines of the nomogram (see insert key in Figure B-1.) This value of predicted loss is then correlated with the measured value to note any degrading effects in the electrical properties of the material.

Dielectric Constant and Loss Tangent of Compound Dielectric Materials. - The relative compound dielectric constant ϵ_m of a mixture of two materials is given empirically by the following relations:

$$\epsilon_m = (\epsilon_1)^a (\epsilon_2)^b \tag{5}$$

$$1 = a + b \tag{6}$$

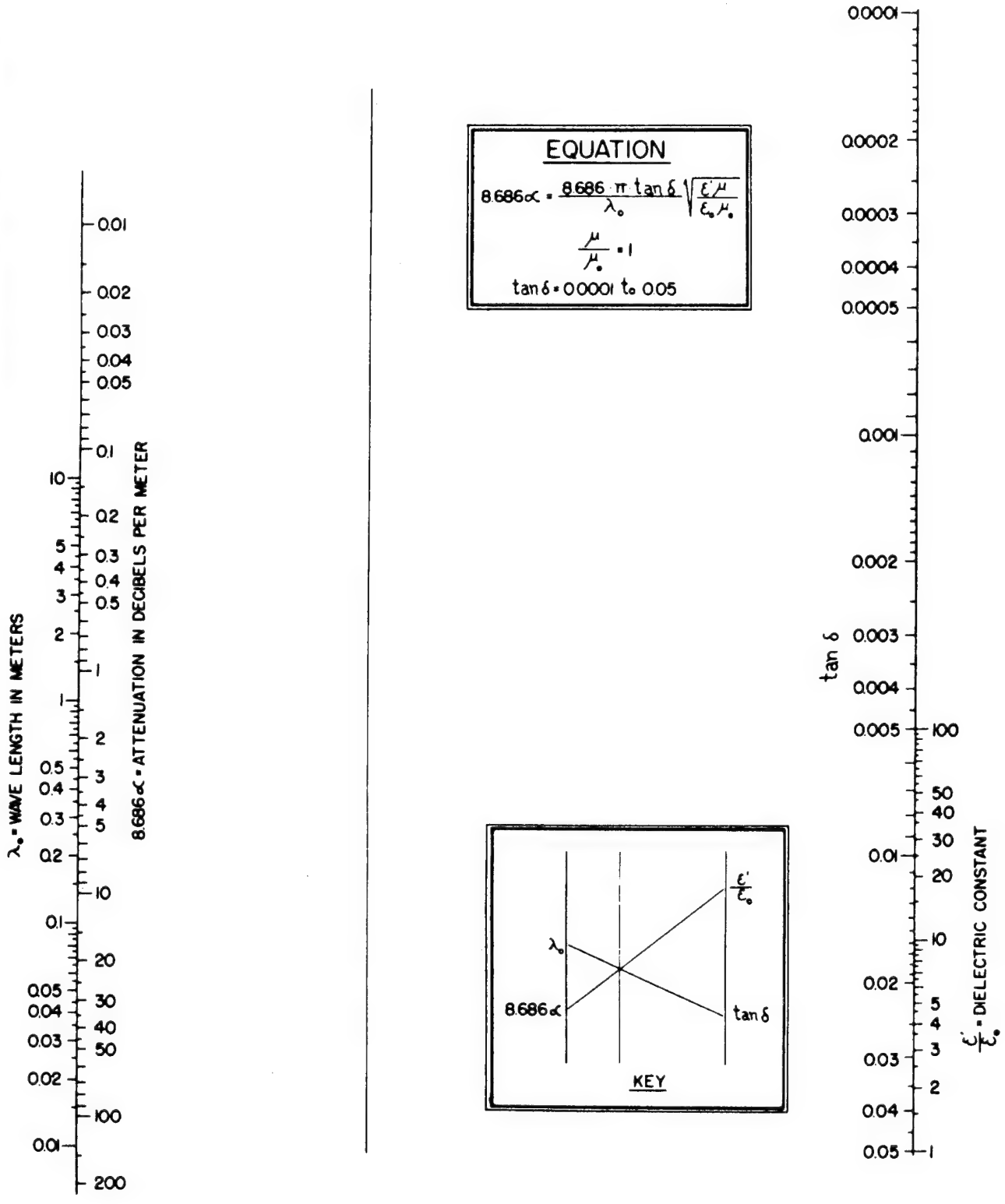

Figure B-1. Nomogram for the Approximate Solution of Equation 4

The terms a and b are the volume fractions of the two component materials and ϵ_1 and ϵ_2 are the respective dielectric constants.

When the energy-absorbing structural material exhibits a rather low dielectric constant due to the incorporation of air into the cell structure, a change in the compound dielectric constant may be related as follows:

$$\epsilon_m = \epsilon_o \left(\frac{\rho_m}{\rho_o}\right) \tag{7}$$

where

ϵ_o = original dielectric constant of the compound open cell material of density ρ_o

ϵ_m = compound dielectric constant of the crushed open cell material of density ρ_m

From equation (2), the loss tangent is related to an effective Q factor of the material. Thus, the compound dielectric loss tangent may be equated through the respective Q factors as follows:

$$\frac{1}{Q_m} = \frac{1}{Q_1} + \frac{1}{Q_2} \tag{8}$$

From equation (2), equation (8) becomes

$$\tan \delta_m = \tan \delta_1 + \tan \delta_2 \tag{9}$$

Taking into account the volume fraction of each material, the loss tangent of a compound dielectric may be approximately equated as follows:

$$\tan \delta_m = a \tan \delta_1 + b \tan \delta_2 \tag{10}$$

As before, for low dielectric air filled cell structures, the equivalent compound loss tangent becomes approximately

$$\tan \delta_m = \left(\frac{\rho_m}{\rho_o}\right) \tan \delta_o \tag{11}$$

where

$\tan \delta_o$ = original loss tangent of the compound open cell material of density ρ_o

$\tan \delta_m$ = loss tangent of the crushed open cell material of density ρ_m

Equations (7) and (11) normally hold for values of ϵ_o less than 1.15 and $\tan \delta_o$ less than 0.005.

APPENDIX C

The honeycomb and the fragmented tube structural elements were determined by the tests conducted in this program to be the most efficient radio frequency transparent structural elements of those evaluated. An additional consideration as part of this program is to determine, within the limits of engineering accuracy, whether the efficiency can be predicted by analytical formulations which would contain the significant material and geometric parameters.

Honeycomb Structural Element. - A method which determines the parameters controlling the crushing stress of a hexagonal cell honeycomb element was presented by McFarland. The method has been verified by experimental results for aluminum honeycomb. A simple mode of collapse of the hexagonal cells was assumed based on experimental observations, and from this the collapse mechanisms were determined. The limit analysis techniques were then applied to the collapse mechanisms, and the energy of deformation computed. The deformation energy was considered to be contributed to by both bending and shear, hence the resulting expression contains a material compression strength, F_{cy}, and also a material shear strength, F_{su}, as follows:

$$\bar{F}_{cc} = F_{cy} (t_c/s)^2 (4.750/K + 28.628) + 1.155 F_{su} (t_c/s) \qquad (1)$$

The above average crushing stress equation contains a K term, an average value of which is considered to be 0.40, and which represents the ratio of one-fourth of a buckling wavelength to the width of a cell wall. By substitution and rearranging equation (1) the new expression is:

$$F_{cc} = (t_c/s) F_{cy} \left[40.503(t_c/s) + 1.155 F_{su}/F_{cy} \right] \qquad (2)$$

The term t_c/s is the ratio of the core foil thickness to cell size which may be expressed in terms of the ratio of core density to material density (ρ_c/ρ)

for hexagonal cells as:

$$t_c/s = (\rho_c/\rho)\ (3/8) \tag{3}$$

substituting equation (3) for the t_c/s terms in equation (2) then:

$$\frac{\bar{F}_{cc}}{\rho_c} = \frac{3}{8}\frac{F_{cy}}{\rho}\ 40.503 \times \frac{3}{8} \times \frac{\rho_c}{\rho} + 1.155\, F_{su}/F_{cy} \tag{4}$$

or

$$\frac{F_{cc}}{\rho_c} = \frac{F_{cy}}{\rho}\left[K_1 \frac{\rho_c}{\rho} + K_2 \frac{F_{su}}{F_{cy}}\right] \tag{5}$$

where $K_1 = 4.69$

$K_2 = 0.433$

The specific energy for a honeycomb element can be determined by considering a cubic element 1 foot on a side. The average crushing load is the crushing stress (F_{cc}) in psi times the loaded area in square inches (144); the stroke is equal to the length of 1 foot and the specific energy is the load times the stroke divided by the weight of the cubic element which is the honeycomb density (ρ_c) in pounds per cubic foot. Then the specific energy absorption capability for honeycomb is:

$$E_{sp} = \frac{144\ \bar{F}_{cc}}{\rho_c} \tag{6}$$

This equation is the same as equation (5) with the addition of 144 as a constant. Then for honeycomb:

$$E_{sp} = \frac{F_{cy}}{\rho}\left[K'_1 \frac{\rho_c}{\rho} + K'_2 \frac{F_{su}}{F_{cy}}\right] \tag{7}$$

where $K'_1 = 675$

$K'_2 = 62.4$

Consider MIL-HDBK-17 phenolic material property values to be representative of nylon phenolic honeycomb material properties for a core

density of 9 lb/ft^3 (ρ_c); material density of 110 per cubic foot (ρ); material compressive strength of 30,000 psi (F_{cy}) (this is actually an ultimate strength (F_{cu}) for fiberglass); material shear to compressive strength ratio (F_{su}/F_{cu}) of 0.316. Then the substitution of these values in equation (7) results in the following:

$$E_{sp} = \frac{30,000}{110}\left[675(9.0/110) + 62.4(0.316)\right]$$

$$E_{sp} = 20,400 \text{ ft-lb/lb}$$

For 75% effective stroke:

$$E_{sp} = 20,400 \times 0.75 = 15,300 \text{ ft-lb/lb.}$$

The actual test values for nylon phenolic honeycomb in 9.0-lb density were 14,400 ft-lb/lb for 3/16-in cell size as reported in Table IV. It is believed that there would be higher values which would approach the 15,000 figure for specimens with the same stroke but of a much larger loaded area, since edge conditions on the specimens tested would reduce the efficiency from the theoretical value. It is concluded that equation (7) is representative of the parameters of fiberglass honeycomb geometry and material properties which define its specific energy absorption capability.

Fragmented Tube Structural Element. - The sequence of events in the fragmenting of a tube over a die may be described first as a hoop expansion of the tube end over the die groove, which represents a lip bursting stress plus a rolling action, which in turn represents a running moment around the circumference of the tube end tending to turn the tube inside out. This action was demonstrated on the vinyl tubing in Figure 8 where these tubes were turned inside out. As the tube is stretched over the die groove, tube friction on the die contributes to the energy absorption process. When the tube is stretched farther to the hoop strength failure stress level, it splits into a series of longitudinal fingers. These fingers are pushed around the die groove causing an additional friction, and the

bending action on these fingers causes fragmenting. The question as to what contributes most to the energy absorption efficiency; i.e., friction before bursting of the tube, friction after the fingers are formed and bent, or fragmenting of the fingers, may be answered by studying test results. Some indication of the significant parameters can be determined by examination of several tubing types retabulated from Table VI. These tubes were all tested on a die with the same radius (r = 0.100).

Weave	Plies Direction	Fragmenting Stress ksi	Tube Hoop Properties				Specific Energy E_{sp} ft-lb/lb
			Modulus $E/10^6$ psi	Strength F_{tu} ksi	Strain e_H in./in.	% r	
181	6L	19.15	3.14	42.4	.0125	6.25	23,800
143	4L	25.00	2.08	10.2	.0490	24.50	28,400
143	4H	11.05	5.12	85.0	.0166	8.30	12,300

This tabulation indicates that the most efficient tube was the longitudinally oriented 143 fabric weave, and that its efficiency is more than twice the efficiency of the hoop direction 143 weave. The %r column is an indication of the distance the tube lip has penetrated by stretching into the die groove of radius r. A comparison between the bi-directional 181 tube and the hoop directional 143 tube shows that the penetrations are similar yet the hoop direction 143 material properties are so much stronger than the 181 hoop properties that if friction before fragmenting were the major contribution, the 143 tube should have been the more efficient. If the assumption is made that the longitudinal bending strength and stiffness of the fingers is the most significant property, then the high efficiency of the 143 fabric longitudinally orientated is proof of this assumption. The limitation on use of longitudinally oriented 143 fabric is that the corresponding hoop strength is so low, consequently when splitting commences it may become a self propagating

crack and the whole tube splits as has happened. The bi-directional 181 fabric, which has a high specific strength, actually represents a more reliable compromise on the use of orthotropic materials for tube fragmenting energy absorption processes.

BIBLIOGRAPHY

McGehee, John R.: A Preliminary Experimental Investigation of An Energy-Absorption Process Employing Frangible Metal Tubing. NASA TN D-1477, Oct 1962.

Reeder, R. B.: Glass Fiber Reinforced Plastics for XQ-10 Development Program. AMC TR No. 59-7-263, ASTIA Document No. AD-156073. Period 12 Oct 1953 to Mar 1959.

Plastics for Flight Vehicles, Part I of Reinforced Plastics, MIL-HDBK-17, 5 Nov 1959.

Duke, W. M.: Lunar Landing Problems. Volume 10 of Advances in the Astronautical Sciences, Section on Manned Lunar Flight. Proceedings of The American Astronautical Society Symposium On Manned Lunar Flight, 29 Dec 1961, Denver.

Hardrath, H. F.: and McEvily, A. J.: Engineering Aspects of Fatigue Crack Propagation. Proceedings of the Crack Propagation Symposium, Vol. I, Cranfield, U. K., 1961.

Coppa, Anthony P.: Collapsible Shell Structures for Lunar Landings. Preprint 2156-61, American Rocket Soc., Oct 1961.

Metallic Materials and Elements for Flight Vehicle Structures, MIL-HDBK-5, Aug 1962.

Mechanical Properties of Hexcel Honeycomb Materials: Hexcel Products Inc., 1 Jan 1964, Revised 20 Feb 1964.

Brooks, G. W. ; and Carden, Huey D.: A Versatile Drop Test Procedure for the Simulation of Impact Environments. Noise Control Shock and Vibration, Vol. 7, No. 5, Sept.-Oct. 1961, pp. 4-8.

Jasik, H.: Antenna Engineering Handbook, McGraw-Hill Book Co. Inc., 1961, pp. 32-30.

Von Hipple, A.: Dielectrics and Waves. John Wiley and Sons, Inc., 1954, page 28.

McFarland, R.K.: A Limit Analysis of the Collapse of Hexagonal Cell Structures under Axial Load. IAS National Summer Meeting, Los Angeles. June 19-22, 1962.